Studying explicit $U(1)_A$ symmetry breaking in a hot and magnetized two flavor nonlocal NJL model constrained using lattice results

Mahammad Sabir Ali [1,*] Chowdhury Aminul Islam [2,1,†] and Rishi Sharma [1,‡]

[1]*Department of Theoretical Physics, Tata Institute of Fundamental Research,*
Homi Bhabha Road, Mumbai 400005, India
[2]*School of Nuclear Science and Technology, University of Chinese Academy of Sciences,*
Beijing 100049, China

We study the two flavor nonlocal Nambu–Jona-Lasinio (NJL) model in the presence of a magnetic field and explore the chiral crossover in presence of a nonlocal form of the 't Hooft determinant term. Its coupling is governed by a dimensionless parameter c. This term is responsible for the explicit breaking of $U(1)_A$ symmetry. We have attempted a systematic analysis of the model parameters by fitting to self-consistent lattice QCD calculations. Three parameters of the model are fixed by $eB = 0$ results from published lattice QCD calculations on the chiral condensate, the pion decay constant (F_π), and the pion mass (m_π). The difference of the u and d quark condensates in the presence of a magnetic field (eB) is quite sensitive to c, and we fix c using published lattice QCD results for this observable. We see no evidence that c depends on eB. The crossover temperature decreases with increasing eB only for condensate values at the lower end of the allowed values [as already seen in V. Pagura *et al.* Phys. Rev. D **95**, 034013 (2017)], and F_π at the upper end of the allowed values. We further check our model predictions by calculating the topological susceptibility with the fitted c values and comparing it with lattice results. Since the topological susceptibility is related to the extent of the $U(1)_A$ symmetry breaking, we find that it is sensitive to the value of c.

I. INTRODUCTION

The study of quantum chromodynamics (QCD) matter in the presence of strong magnetic fields is a topic of current interest (see [1] for a broad review). Phenomenologically, it is interesting because a strong magnetic field is present in the initial stages of heavy ion collisions (HICs) ($\sim 15m_\pi^2; m_\pi^2 \approx 10^{18}$ G) [2,3]. Intense fields in the range 10^{14}–10^{19} G may also exist in the core of magnetars [4].

The QCD phase diagram in the presence of magnetic fields, particularly the chiral crossover, has been heavily studied for the last few decades. From different effective QCD model investigations [5–13] and from the earliest lattice QCD study [14], it was generally believed that at zero chemical potential the value of the chiral condensate at any temperature T in the presence of a magnetic field will be larger than its value at $eB = 0$. This property is termed as magnetic catalysis (MC).

With more controlled lattice calculations [15,16] the chiral condensate was found to decrease with an increasing magnetic field near the crossover temperature. This behavior was termed as inverse magnetic catalysis (IMC). These effects have been studied for various magnetic fields and m_π [15–19]. This sharper reduction in the condensate in the crossover region often leads to a reduction of the crossover temperature with increasing eB, which we will also loosely call the IMC effect below. (A reduction in the crossover temperature does not imply the IMC effect for m_π significantly larger than the physical π mass [18].)

Since IMC was discovered using lattice QCD, several attempts have been made to understand it through effective QCD models [20–33]. A family of local Nambu–Jona-Lasinio [34,35] (NJL) models explains the IMC by incorporating the effect of the energy scale eB on the four fermion coupling. The motivation for this choice is that in QCD the presence of this additional energy scale is expected to weaken the coupling as eB increases. Modeling this effect by reducing the four Fermi interaction strength with eB leads to IMC in the crossover region.

The NJL interaction is local, which makes the model simple yet powerful. The price paid for the model's

*sabir@theory.tifr.res.in
†chowdhury.aminulislam@gmail.com
‡rishi@theory.tifr.res.in

simplicity is the fact that the results of observables might depend on the regularization procedure used. The most popular regularization used is the introduction of a three momentum cutoff. In this scheme, the QCD interaction is assumed to be constant up to the value of the cutoff, and modes above the cutoff are dropped. This procedure misses the important nature of running of QCD coupling constant with energy, and hence, the reduction in the coupling constant as a function of eB needs to be put in by hand.

The nonlocal [36–40] version of the NJL model is introduced to overcome some of the above-mentioned drawbacks of the local NJL model. Technically, the resulting expressions for the observables in the theory are similar to implementing a soft cutoff using form factors that decrease with increasing momenta but the intuition is more than that. The reduction of the quark interaction with increasing energy qualitatively mimics the nature of the running of the QCD coupling constant. The nonlocal version of the model also describes spontaneous chiral symmetry breaking. Some aspects of confinement have also been described in the model [36,37].

The nonlocal version of the NJL model has been used to describe QCD matter under strong magnetic field. In contrast to the standard NJL model (where one needs to use multiple fitted parameters [21,22]), it naturally leads to the effect of IMC [33] without using a four Fermi interaction that explicitly depends on eB. To keep note of the chronology of the actual development, it should be mentioned here that the first attempt of incorporation of a magnetic field in nonlocal NJL model showed MC at all temperatures [41]. There the magnetic field was introduced just like what is usually done in the local NJL model. On the other hand, in Ref. [33], the analysis was performed following a more rigorous procedure based on the Ritus eigenfunction method [42] with the inclusion of a nonlocal quark model with separable interactions including a coupling to a uniform magnetic field. Our choice of working with this model particularly stems from this important fact that it naturally shows the IMC effect near crossover, in agreement with lattice results.

Here we build upon the work of Refs. [33,43] and study the two flavor nonlocal NJL model in presence of a magnetic field to explore the chiral phase transition. In this paper, we will focus on the Gaussian form factor, which is one of the two considered by Refs. [33,43].

The first addition to Refs. [33,43] is that we add to the nonlocal form of the standard four Fermi NJL interaction, the 't Hooft determinant term with an arbitrary coupling constant. The usual NJL interaction has the well-known form,

$$\frac{G_0}{2}[(\bar{\psi}\psi)^2 + (\bar{\psi}i\gamma^5\tau^a\psi)^2], \qquad (1)$$

which can be written as the sum of $U(1)_A$ symmetric term [$\mathcal{L}_1$ in Eq. (4) below] and a $U(1)_A$ breaking 't Hooft determinant term [$\mathcal{L}_2$ in Eq. (5) below] with equal coupling. The 't Hooft determinant term arises due to instantons and is included in such effective QCD models to break the $U(1)_A$ symmetry, which mimics the axial anomaly in QCD. The difference between the two couplings is governed by the dimensionless parameter c [defined in Eq. (7) below]. For $c = 1/2$, the strength of the two couplings are equal, and the interaction is of the form Eq. (1). References [33,43] considered the nonlocal generalization of this case. By allowing the two couplings to be independent ($c \neq 1/2$), the sum of the u and d quark condensates and the difference of the u and d quark condensates are governed by two independent coupling constants.

In the absence of any isospin symmetry breaking, the u and d condensates are equal (we assume $m_u = m_d$) and so are the respective constituent quark masses. The value of c does not play any role as only the sum of the u and d condensates is nontrivial.

If one considers nonzero isospin chemical potential (μ_I [44]) or/and magnetic field (eB [9]), the independent appearance of both the u and d quark condensates in the u and d constituent masses become important. This effect has been termed as "flavor mixing" [44] in the literature (although "flavor coupling" might be a more appropriate term). This "flavor mixing" depends on c.

These facts make the consideration of an arbitrary strength of 't Hooft interaction in the presence of a magnetic field quite relevant. With these combined effects of instantons and magnetic field, the exploration becomes more interesting. On one hand, the "flavor mixing" effects coming via the instantons try to restore the isospin symmetry, and on the other hand, the strength of the magnetic field breaks it further as the different flavors couple with the magnetic field with different strengths [9].

One important result of our analysis is that an eB independent c describes the lattice results for the u, d condensate difference at $T = 0$ quite well, and this allows us to extract the value of c using lattice results on the u, d condensate difference. Results for the thermodynamics of isosymmetric matter cannot be used to constrain c. To our knowledge, this is the first attempt to constrain c using lattice results.

The results of [32,33] for the u, d condensate difference at $T = 0$ as a function of eB with $c = 1/2$ agree quite well with the lattice results when the model is fitted to a larger value of the sum of the u, d condensate at $eB = 0$. However, the condensate differences for different values of the magnetic field, have not been contrasted against the lattice QCD data for finite T. Here, we aim to compare our findings for both zero and nonzero temperature with the lattice data with c fitted to $T = 0$ results.

Our second addition is a more systematic analysis of the parameters of the model by fitting to a self-consistent set of lattice results. The pertinent parameters for $eB = 0$ in the nonlocal NJL model are the overall four Fermi coupling

strength G_0, the "cutoff" Λ (which determines the momentum beyond which the form factor drops rapidly), and the bare quark mass m. These are usually [45,46] fitted to match F_π, m_π and the condensate $\langle \bar{\psi}\psi \rangle$, and we follow the same procedure. (Recall that c does not play a role for $eB = 0$.) While F_π, m_π are very well constrained from experiments and lattice [47], the condensate value is often taken from models or phenomenology.

In Ref. [33], it has already been demonstrated that IMC in the crossover region is seen only for smaller values of the chiral condensate within a physically motivated range of values [Ref. [33] considered a range of values of $(\langle \bar{\psi}\psi \rangle)^{1/3}$ from 210 MeV to 240 MeV.], especially for the Gaussian form factor.

In this paper, we fit the model to self-consistent calculations of the chiral condensate and F_π for realistic m_π, on the lattice. We consider the parameter set by the JLQCD Collaboration, with the central value of condensate being $\langle \bar{\psi}_f\psi_f \rangle^{1/3} = 240$ MeV [48] (at the renormalization scale 2 GeV, see Sec. III A). We denote a specific flavor f (u or d) of the ψ as ψ_f. When f is summed over, we denote the bilinear as $\bar{\psi}\psi$. To increase the exploration range in the space of the chiral condensate, we consider another LQCD calculation [49], for which the value of the condensate is a bit larger ($\langle \bar{\psi}_f\psi_f \rangle^{1/3} = 261$ MeV). From this inclusion, it becomes evident that within such effective models, the IMC effect can only be observed for smaller values of chiral condensates. This corroborates the findings in Ref. [33]. We put the whole discussion related to the second lattice data in Appendix B.

Like Ref. [33], we also find that within the error band of $\langle \bar{\psi}_f\psi_f \rangle^{1/3}$ IMC is obtained for the condensates near the lower edge of the range. In addition, we find that within the error band of F_π to get a better match with the phase diagram given by LQCD [15], one needs to consider F_π towards the upper edge of the range. Our analysis clearly indicates that the obtainment of the IMC effect in such a nonlocal effective QCD model also depends on the values of F_π.

In addition to the above two improvements, the inclusion of the parameter c presents us with the scope of exploring the temperature evolution of the axial anomaly breaking term. In particular, it is expected that the $U(1)_A$ symmetry gets restored at high enough temperature, estimated to be near or above the chiral crossover temperature [50]. Here, the investigation becomes more interesting in the presence of a magnetic field, which breaks the isospin symmetry as well. One observable that can be impacted by a finite c is the topological susceptibility (χ_t), and we also calculate it as a function of eB and T for the fitted values of the parameters. χ_t has been calculated for the local NJL model for physically motivated values of c before [51,52]. We now calculate this in the nonlocal case and compare it with lattice calculations, which helps to provide an extra check on our model.

We organize the paper as follows: In Sec. II, we briefly review the formalism for the model used in this article. We start the discussion by considering the instanton term at zero temperature and magnetic field in nonlocal model and subsequently, in Sec. II A, we shift the focus to the scenario for nonzero temperature and magnetic field. In Sec. II B, we give a brief description for the topological susceptibility. Then in Sec. III, the results of the paper have been outlined. In Sec. III A, we give details of the fitting of the model parameters and the necessary criteria. We show the results for the fitting of the $U(1)_A$ symmetry breaking parameter c at zero eB and T in Sec. III B. In Sec. III C, we show the model prediction for condensate average, phase diagram and condensate difference with the fitted c value and compare them with the available LQCD results. We further show the model predictions for χ_t with the fitted c values along with the comparison with LQCD results in Sec. III D. Finally, in Sec. IV, we conclude.

To avoid breaking the flow of the paper, we have moved some material to the Appendix. In Appendix A, the dependence of the mass of (2 flavors) $U(1)_A$ fluctuations on c is shown. In Appendix B, results for Brandt13 are discussed. Finally, in Appendix C, the dependence of χ_t on c is discussed.

II. FORMALISM

In this section, we briefly discuss the formalism used in the nonlocal NJL model. As mentioned earlier, our main goal is to study the interplay between the effect of the magnetic field and the 't Hooft determinant term, particularly the interplay of the magnetic field with the strength of the explicit axial symmetry breaking.

In the standard NJL model, the strengths of axial symmetric and axial symmetry breaking interaction terms are equal [45,46]. We follow the prescription of Ref. [44], where they have considered a general NJL Lagrangian with arbitrary interaction strengths for $U(1)_A$ symmetric and breaking interactions,

$$\mathcal{L}_{\text{NJL}} = \mathcal{L}_0 + \mathcal{L}_1 + \mathcal{L}_2, \tag{2}$$

where the kinetic term is

$$\mathcal{L}_0 = \bar{\psi}(i\slashed{\partial} - m)\psi, \tag{3}$$

and the interactions are given by

$$\mathcal{L}_1 = G_1\{(\bar{\psi}\psi)^2 + (\bar{\psi}\vec{\tau}\psi)^2 + (\bar{\psi}i\gamma_5\psi)^2 + (\bar{\psi}i\gamma_5\vec{\tau}\psi)^2\} \text{ and} \tag{4}$$

$$\mathcal{L}_2 = G_2\{(\bar{\psi}\psi)^2 - (\bar{\psi}\vec{\tau}\psi)^2 - (\bar{\psi}i\gamma_5\psi)^2 + (\bar{\psi}i\gamma_5\vec{\tau}\psi)^2\}, \tag{5}$$

with $\mathcal{L}_1$ being symmetric under $U(1)_A$, but $\mathcal{L}_2$ is not. $\vec{\tau}$ represents Pauli matrices.

In the absence of isospin chemical potential (μ_I) and magnetic field (eB) (we take $m_u = m_d$), the chiral condensate,

$$\langle \bar{\psi}(x)\psi(x)\rangle, \tag{6}$$

spontaneously breaks the (approximate) $SU(2)_A$ symmetry. In mean field theory, it depends only on the combination $(G_1 + G_2)$. The state is $SU(2)_V$ symmetric.

In the presence of μ_I or/and eB as the $SU(2)_V$ symmetry is explicitly broken, one can have $\langle \bar{\psi}\tau_3\psi\rangle$ condensate, which depends also on the combination $(G_1 - G_2)$. We can parametrize the coupling constants as

$$G_1 = (1 - c)G_0/2$$
$$G_2 = cG_0/2, \tag{7}$$

where $c = 1/2$ corresponds to the usual NJL model.

The local version of the NJL model lacks some important features of the full QCD theory. For example, asymptotic freedom, momentum dependent constituent mass, etc. To implement these features in NJL type models qualitatively, one may consider the nonlocal version of it. With a nonlocal form factor, one can qualitatively incorporate the idea of asymptotic freedom in the NJL model.

The nonlocal NJL Lagrangian has the same structure as Eq. (2), where the interaction term can be written as [32,33,36–40,43],

$$\mathcal{L}_1 = G_1\{j_a(x)j_a(x) + \tilde{j}_a(x)\tilde{j}_a(x)\} \quad \text{and}$$
$$\mathcal{L}_2 = G_2\{j_a(x)j_a(x) - \tilde{j}_a(x)\tilde{j}_a(x)\}.$$

Here, $j_a(x)$ and $\tilde{j}_a(x)$ are the nonlocal currents, given by (scheme II) [43]

$$j_a(x)/\tilde{j}_a(x) = \int d^4z \mathcal{H}(z)\bar{\psi}\left(x + \frac{z}{2}\right)\Gamma_a/\tilde{\Gamma}_a\psi\left(x - \frac{z}{2}\right), \tag{8}$$

where $\Gamma_a = (\mathbb{I}, i\gamma_5\vec{\tau})$, $\tilde{\Gamma}_a = (i\gamma_5, \vec{\tau})$ with $a = \{0, 1, 2, 3\}$, and $\mathcal{H}(z)$ is the nonlocal form factor in position space.

For the rest of this subsection, let us assume that the isospin is a symmetry of the system (neither μ_I nor eB is present). With $G_2 \neq 0$ in the chiral limit, the symmetry of the above Lagrangian is

$$SU(2)_V \times SU(2)_A \times U(1)_V. \tag{9}$$

With $G_2 = 0$, it has an additional $U_A(1)$ symmetry.

The next step is to integrate out the fermionic degrees of freedom. To do that, moving to the Euclidean space from the Minkowski space will make the calculation easier. This can be achieved with the help of Wick rotation, which can be performed through the following transformations:

$$t \to -ix_4 \quad \text{and} \quad \gamma_0 \to i\gamma_4. \tag{10}$$

With the metric $g_{\mu\nu} = \text{diag}(-1, -1, -1, -1)$, all the calculations done below are in Euclidean space.

To integrate out the fermionic degrees of freedom, one needs to linearize the theory, which can be done with the help of Hubbard–Stratonovich (HS) transformation. In the HS transformation, one can introduce four auxiliary fields associated with the four different types of interactions. For a detailed bosonization calculation, one can look in the Appendix A of Ref. [53]. We mark the isoscalar and isovector auxiliary fields by σ and π, respectively, and use "s" and "ps" in the subscripts to denote Lorentz scalar and pseudoscalar, respectively. In a mean-field approximation, some of the auxiliary fields have an equilibrium expectation value.

The expectation value of operators in the pseudoscalar channel is 0 due to parity conservation. In the absence of μ_I and eB, isospin symmetry ensures

$$\langle \bar{\psi}(x)\vec{\tau}\psi(x)\rangle = 0. \tag{11}$$

This makes the free energy (Ω) and other vacuum observables independent of c.

The auxiliary field σ_s is given by

$$\sigma_s(x) = -\frac{G_0}{2}\int d^4z \mathcal{H}(z)\bar{\psi}\left(x + \frac{z}{2}\right)\psi\left(x - \frac{z}{2}\right). \tag{12}$$

With only the nonzero scalar-isoscalar auxiliary field, one gets the mean-field Lagrangian as

$$\mathcal{L}_{\text{MF}} = \bar{\psi}(x)\left(\delta^4(x - y)(-i\not{\partial} + m) + \mathcal{H}(x - y)\sigma_s\left(\frac{x + y}{2}\right)\right)$$
$$\times \psi(y) + \frac{1}{2G_0}\sigma_s^2\left(\frac{x + y}{2}\right). \tag{13}$$

Assuming that the mean-field is homogeneous and isotropic (for $eB = 0$) throughout space and time, we take σ_s in Eq. (12) independent of x. With the above assumption, one can obtain the formal expression for the free energy per unit volume as

$$\Omega = \frac{S_{\text{MF}}}{V^{(4)}} = -2N_fN_c\int \frac{d^4q}{(2\pi)^4}\ln[q^2 + M^2(q)] + \frac{\sigma_s^2}{2G_0}. \tag{14}$$

In the mean field approximation, the constituent quark mass is given by

$$M(q) = m + h(q, q)\sigma_s. \tag{15}$$

$h(p, p')$ is the nonlocal form factor in momentum space, the Fourier transformation of $\mathcal{H}(x - y)$. It is function of only $p + p'$ as one can see from Eq. (13).

We follow the procedure used in Ref. [43] and consider the nonlocal form factor to be Gaussian. The explicit form is

$$h(p, p') = e^{-(p+p')^2/(4\Lambda^2)}. \tag{16}$$

The self-consistent gap equation has the following form:

$$\sigma_s = 8N_c G_0 \int \frac{d^4q}{(2\pi)^4} h(q, q) \frac{M(q)}{q^2 + M^2(q)}. \tag{17}$$

With σ_s given by Eq. (17), one can calculate the formal expression for the local condensate by differentiating the Ω with respect to current quark mass as

$$\langle \bar{\psi}_f(x)\psi_f(x) \rangle = \frac{\partial \Omega}{\partial m} = -4N_c \int \frac{d^4q}{(2\pi)^4} \frac{M(q)}{q^2 + M^2(q)}. \tag{18}$$

We note that the right-hand side in Eq. (18) is not convergent away from the chiral limit [substituting $m = 0$ in Eq. (15) implies that $M(p) \to 0$ at large p] and needs to be regularized. This can be done by subtracting the identical expression with $M = m$. This prescription can be understood from Eq. (14) if we subtract the analogous term from the formal expression of the free energy to make it regular.

Now, to fit the model parameters, we use pion mass and also pion decay constant. To get the pion mass, we need to calculate the pion propagator which can be obtained from the quadratic term in the pionic fluctuation from the bosonized action as

$$G^{\pm}(p^2) = \frac{1}{G_0} - 8N_c \int \frac{d^4q}{(2\pi)^4} h^2(q^+, q^-)$$
$$\times \frac{[(q^+ \cdot q^-) \mp M(q^+)M(q^-)]}{[(q^+)^2 + M^2(q^+)][(q^-)^2 + M^2(q^-)]}, \tag{19}$$

where $+$ sign in $G^{\pm}$ corresponds to the σ mode and $-$ sign to the pionic mode with $q^{\pm} = q \pm p/2$. The pion mass is obtained from

$$G^{-}(-m_\pi^2) = 0. \tag{20}$$

Following the steps given in Ref. [43], we use the expression for pion decay constant,

$$m_\pi^2 F_\pi = m Z_\pi^{1/2} J(-m_\pi^2), \tag{21}$$

where $J(p^2)$ given by

$$J(p^2) = 8N_c \int \frac{d^4q}{(2\pi)^4} h(q^+, q^-)$$
$$\times \frac{[(q^+ \cdot q^-) + M(q^+)M(q^-)]}{[(q^+)^2 + M^2(q^+)][(q^-)^2 + M^2(q^-)]}, \tag{22}$$

and Z_π is related to the $\pi \bar{\psi}_f \psi_f$ coupling constant and is given by

$$Z_\pi^{-1} = \frac{dG^{-}(p)}{dp^2}\bigg|_{p^2 = -m_\pi^2}. \tag{23}$$

Equations (35), (20), and (21) are used to fit the free parameters of the model, m (current quark mass), G_0 and Λ with a given form factor. In the case of the Gaussian form factor, Λ characterizes the range of nonlocal interaction. In other words, it controls at what scale the coupling starts becoming small. These parameters are fitted to obtain a phenomenologically allowed quark condensate, physical pion mass, and pion decay constant.

A. Nonzero temperature and magnetic field

To include both the temperature and magnetic field, we follow the procedure given in Ref. [33]. Since the isospin $SU(2)$ symmetry (both vector and axial) is broken in the presence of a magnetic field, we introduce another auxiliary field π_s [9]. Pseudoscalar mean fields are still not allowed due to the parity symmetry.

Introducing these two auxiliary fields (σ_s, π_s, introduced in the previous section), one can obtain the effective Euclidean action using the mean field Lagrangian,

$$S_{\text{bos}} = -\ln \det \mathcal{D} + \frac{1}{2G_0} \int d^4x \sigma_s^2(x)$$
$$+ \frac{1}{2(1 - 2c)G_0} \int d^4x \vec{\pi}_s(x) \cdot \vec{\pi}_s(x), \tag{24}$$

where the fermionic determinant is given by

$$\mathcal{D}\left(x + \frac{z}{2}, x - \frac{z}{2}\right) = \gamma_0 W\left(x + \frac{z}{2}, x\right) \gamma_0 [\delta^{(4)}(z)(-i\partial\!\!\!/ + m)$$
$$+ \mathcal{H}(z)[\sigma_s(x) + \vec{\tau} \cdot \vec{\pi}_s(x)]] W\left(x, x - \frac{z}{2}\right). \tag{25}$$

Here, $W(x, y)$ is given as $W(x, y) = P\exp[-i\hat{Q} \int_x^y dr_\mu \mathcal{A}_\mu(r)]$. As for the nonmagnetic field scenario, here also we will assign space-time independent mean field values to the auxiliary fields. Without loss of generality, we can choose $\vec{\pi}_s$ to be in the τ^3 (π_s^3) direction. As already mentioned, all other pseudoscalar auxiliary fields are chosen to have zero mean field values. Then the fermionic determinant and the action become

$$\mathcal{D}^{\mathrm{MFA}}(x, x') = \delta^{(4)}(x - x')(-i\not{\partial} - \hat{Q}Bx_1\gamma_2 + m)$$

$$+ (\sigma_s + \tau_3\pi_s^3)\mathcal{H}(x - x')\exp\left[\frac{i}{2}\hat{Q}B(x_2 - x_2')(x_1 + x_1')\right] \quad \text{and} \tag{26}$$

$$S_{\mathrm{bos}} = -\ln\det\mathcal{D}^{\mathrm{MFA}} + \frac{1}{2G_0}\int d^4x\sigma_s^2 + \frac{1}{2(1 - 2c)G_0}\int d^4x(\pi_s^3)^2, \tag{27}$$

respectively.

Following the Ritus eigenfunction method [42] as employed in Ref. [33], we obtain the constituent mass for a Gaussian nonlocality form factor as

$$M_{q_\parallel,k}^{\lambda,f} = m + (\sigma_s + s_f\pi_s^3)\frac{(1 - |q_fB|/\Lambda^2)^{k + \frac{\lambda s_f - 1}{2}}}{(1 + |q_fB|/\Lambda^2)^{k + \frac{\lambda s_f + 1}{2}}}\exp(-q_\parallel^2/\Lambda^2), \tag{28}$$

where $q_\parallel = (q_3, q_4)$, $s_f = \mathrm{sign}(q_f)$, k is the Landau level index and $\lambda = \pm 1$ is the spin. The free energy per unit volume is given by

$$\Omega = \frac{S_{\mathrm{bos}}^{\mathrm{MFA}}}{V^{(4)}} = \frac{\sigma_s^2}{2G_0} + \frac{(\pi_s^3)^2}{2(1 - 2c)G_0} - N_c\sum_{f=u,d}\frac{|q_fB|}{2\pi}\int\frac{d^2q_\parallel}{(2\pi)^2}\left\{\ln\left[q_\parallel^2 + (M_{q_\parallel,0}^{s_f,f})^2\right]\right.$$

$$\left. + \sum_{k=1}^{\infty}\ln\left[(2k|q_fB| + q_\parallel^2 + M_{q_\parallel,k}^{-1,f}M_{q_\parallel,k}^{+1,f})^2 + q_\parallel^2(M_{q_\parallel,k}^{+1,f} - M_{q_\parallel,k}^{-1,f})^2\right]\right\}. \tag{29}$$

The two gap equations can be obtained by differentiating the above equation with respect to σ_s and π_s^3 as

$$\frac{\partial\Omega}{\partial\sigma_s} = \frac{\sigma_s}{G_0} - N_c\sum_{f=u,d}\frac{2|q_fB|}{2\pi}\int\frac{d^2q_\parallel}{(2\pi)^2}\left\{\frac{M_{q_\parallel,0}^{s_f,f}A_{q_\parallel,0}^{s_f,f}}{q_\parallel^2 + (M_{q_\parallel,0}^{s_f,f})^2}\right.$$

$$+ \sum_{k=1}^{\infty}\left[\frac{(2k|q_fB| + q_\parallel^2 + M_{q_\parallel,k}^{-1,f}M_{q_\parallel,k}^{+1,f})(A_{q_\parallel,k}^{-1,f}M_{q_\parallel,k}^{+1,f} + M_{q_\parallel,k}^{-1,f}A_{q_\parallel,k}^{+1,f})}{(2k|q_fB| + q_\parallel^2 + M_{q_\parallel,k}^{-1,f}M_{q_\parallel,k}^{+1,f})^2 + q_\parallel^2(M_{q_\parallel,k}^{+1,f} - M_{q_\parallel,k}^{-1,f})^2}\right.$$

$$\left.\left. + \frac{q_\parallel^2(M_{q_\parallel,k}^{+1,f} - M_{q_\parallel,k}^{-1,f})(A_{q_\parallel,k}^{+1,f} - A_{q_\parallel,k}^{-1,f})}{(2k|q_fB| + q_\parallel^2 + M_{q_\parallel,k}^{-1,f}M_{q_\parallel,k}^{+1,f})^2 + q_\parallel^2(M_{q_\parallel,k}^{+1,f} - M_{q_\parallel,k}^{-1,f})^2}\right]\right\} = 0 \quad \text{and} \tag{30}$$

$$\frac{\partial\Omega}{\partial\pi_s^3} = \frac{\pi_s^3}{(1 - 2c)G_0} - N_c\sum_{f=u,d}s_f\frac{2|q_fB|}{2\pi}\int\frac{d^2q_\parallel}{(2\pi)^2}\left\{\frac{M_{q_\parallel,0}^{s_f,f}A_{q_\parallel,0}^{s_f,f}}{q_\parallel^2 + (M_{q_\parallel,0}^{s_f,f})^2}\right.$$

$$+ \sum_{k=1}^{\infty}\left[\frac{(2k|q_fB| + q_\parallel^2 + M_{q_\parallel,k}^{-1,f}M_{q_\parallel,k}^{+1,f})(A_{q_\parallel,k}^{-1,f}M_{q_\parallel,k}^{+1,f} + M_{q_\parallel,k}^{-1,f}A_{q_\parallel,k}^{+1,f})}{(2k|q_fB| + q_\parallel^2 + M_{q_\parallel,k}^{-1,f}M_{q_\parallel,k}^{+1,f})^2 + q_\parallel^2(M_{q_\parallel,k}^{+1,f} - M_{q_\parallel,k}^{-1,f})^2}\right.$$

$$\left.\left. + \frac{q_\parallel^2(M_{q_\parallel,k}^{+1,f} - M_{q_\parallel,k}^{-1,f})(A_{q_\parallel,k}^{+1,f} - A_{q_\parallel,k}^{-1,f})}{(2k|q_fB| + q_\parallel^2 + M_{q_\parallel,k}^{-1,f}M_{q_\parallel,k}^{+1,f})^2 + q_\parallel^2(M_{q_\parallel,k}^{+1,f} - M_{q_\parallel,k}^{-1,f})^2}\right]\right\} = 0, \tag{31}$$

respectively. Here, $A_{q_\parallel,k}^{\lambda,f}$ is given by

$$A_{q_\parallel,k}^{\lambda,f} = \frac{(1 - |q_fB|/\Lambda^2)^{k + \frac{\lambda s_f - 1}{2}}}{(1 + |q_fB|/\Lambda^2)^{k + \frac{\lambda s_f + 1}{2}}}\exp(-q_\parallel^2/\Lambda^2). \tag{32}$$

The finite temperature is introduced using the Matsubara formalism, which connects the Euclidean time component to the temperature as follows:

$$\int \frac{dq_4}{2\pi} f(q_4) = T \sum_{n=-\infty}^{\infty} f(\omega_n), \qquad (33)$$

where the Mastubara frequency (ω_n) for fermions are given by $\omega_n = (2n+1)\pi T$.

With the above prescription [Eq. (33)], $q_\parallel^2$ is replaced by $(q_3^2 + \omega_n^2)$ in Eqs. (28), (29), (30), and (31); and the integration $\int \frac{d^2 q_\parallel}{(2\pi)^2}$ is replaced by $T \sum_{n=-\infty}^{\infty} \int \frac{dq_3}{(2\pi)}$. Here, we would like to highlight the major difference with the standard NJL model scenario, where one can separate out the vacuum and thermal contribution coming from the fermionic determinant. There the temperature appears only through the momentum component q_4 in the propagator, and using a summation identity, one can easily separate out the above-mentioned two components. In the nonlocal case, however, we cannot separate out the vacuum and the thermal contributions. In the presence of a nonlocal form factor, one gets an explicit temperature dependence in the constituent mass which then prevents us from making any further analytic simplification, and the Matsubara sums needs to be performed numerically.

One can easily notice that the free energy form [Eq. (29)] is divergent due to the integration over q_3. Our purpose is to minimize the free energy and obtain the associated mean field values. To remove the divergence from the action, we can subtract from Eq. (29) the same expression with constituent mass (M) being replaced by the current mass (m). This replacement does not affect the position of the extremum in the mean field space but removes the divergence. The subtraction also ensures that the summations over Landau levels and Matsubara frequencies converge.

The values of the mean fields can be obtained by solving the gap equations. Now if we look into the gap equations [(30) and (31)], we can see that the integrands are multiplied by $A_{q_\parallel,k}^{\lambda,f}$, which goes to zero as $q_3 \to \infty$ due to the exponential factor. Hence, the gap equations are also

divergence free. The same exponential factor makes sure that the summation over Matsubara frequencies converges too, whereas the Landau level summation converges as the effective power of k is -1 with a suppressing factor in the numerator coming from Eq. (32).

Using the two gap equations [(30), (31)], we obtain the mean field values σ_s and π_s^3. σ_s is proportional to the average of u and d condensates and π_s^3 to the difference of them and since $\pi_s^3 = 0$ for $eB = 0$, we expect that for eB small enough,

$$\text{abs}(\sigma_s) \geq \text{abs}(\pi_s^3). \qquad (34)$$

Now looking at the Euclidean action [Eq. (29)] in the chiral limit ($m = 0$) without the mean-field part (i.e., terms one and two on the right-hand side), one observes that it is symmetric under the interchange of σ_s and π_s^3. Then it becomes important to know what guarantees a higher numerical value to σ_s solution compared to π_s^3 and not vice versa. Where a smaller solution for σ_s compared to π_s^3 simply implies that the sign of u and d condensates are different, which is unphysical. This symmetry is broken by the mean field terms. $c \neq 0$ breaks this symmetry, and in the chiral limit, we found out that with $c > 0$, we always end up with physically acceptable solutions, but for $c < 0$, we do not. Hence, $c = 0$ is the boundary line between these two scenarios.

The introduction of a small quark mass (m) shifts this boundary to a slightly negative value in c. Motivated by this discussion, we will restrict ourselves to $c > 0$. We will further see that $c > 1/2$ can be ruled out of other physical considerations, and hence, we shall restrict ourselves to $c \in [0, 1/2]$.

The formal expression for the quark condensate for individual flavors (u and d) can be obtained by differentiating the action with respect to the corresponding current quark mass as before,

$$\langle \bar{\psi}_f \psi_f \rangle = -N_c \sum_{f=u,d} \frac{2|q_f B|}{2\pi} \int \frac{d^2 q_\parallel}{(2\pi)^2} \left\{ \frac{M_{q_\parallel,0}^{s_f,f}}{q_\parallel^2 + (M_{q_\parallel,0}^{s_f,f})^2} + \sum_{k=1}^{\infty} \frac{(2k|q_f B| + q_\parallel^2 + M_{q_\parallel,k}^{-1,f} M_{q_\parallel,k}^{+1,f})(M_{q_\parallel,k}^{+1,f} + M_{q_\parallel,k}^{-1,f})}{(2k|q_f B| + q_\parallel^2 + M_{q_\parallel,k}^{-1,f} M_{q_\parallel,k}^{+1,f})^2 + q_\parallel^2 (M_{q_\parallel,k}^{+1,f} - M_{q_\parallel,k}^{-1,f})^2} \right\}. \qquad (35)$$

In the large-p region, one easily find out that the above integral is divergent with nonzero quark masses. To obtain a finite condensate, one need to regularize it. Here, we have used the same regularization procedure as used in Ref. [33],

$$\langle \bar{\psi}_f \psi_f \rangle_{B,T}^{\text{reg}} = \langle \bar{\psi}_f \psi_f \rangle_{B,T} - \langle \bar{\psi}_f \psi_f \rangle_{B,T}^{\text{free}} + \langle \bar{\psi}_f \psi_f \rangle_{B,T}^{\text{free,reg}}, \qquad (36)$$

where "free" implies that there is no self-interaction and $\langle \bar{\psi}_f \psi_f \rangle_{B,T}^{\text{free,reg}}$ is given by

$$\langle \bar{\psi}_f \psi_f \rangle_{B,T}^{\text{free,reg}} = \frac{N_c m^3}{4\pi^2} \left[\frac{\ln \Gamma(x_f)}{x_f} - \frac{\ln(2\pi)}{2x_f} + 1 - \left(1 - \frac{1}{2x_f} \ln x_f\right) \right] + \frac{N_c |q_f B|}{\pi} \sum_{k=0}^{\infty} \alpha_k \int \frac{dq}{2\pi} \frac{m}{E_k^f (1 + \exp[E_k^f / T])}, \qquad (37)$$

with $x_f = m^2/(2|q_f B|)$. It is obvious that the "free,reg" term will be zero in absence of magnetic field.

Finally, to compare our findings with LQCD results [16], we use their definition of the renormalized condensate, which was used to cancel both additive and multiplicative divergences that appear in the lattice calculation. The form is given below,

$$\Sigma_{B,T}^f = \frac{2m}{\mathcal{N}^4} [\langle \bar{\psi}_f \psi_f \rangle_{B,T}^{\text{reg}} - \langle \bar{\psi}_f \psi_f \rangle_{0,0}^{\text{reg}}] + 1, \quad (38)$$

where $\mathcal{N}$ is given by $\mathcal{N} = (m_\pi F_{\pi,0})^{1/2}$, which follows from Gell-Mann-Oakes-Renner (GOR) relation, m_π is the neutral pion mass, and $F_{\pi,0}$ is the pion decay constant in the chiral limit.

B. Topological susceptibility (χ_t)

The QCD Lagrangian features a CP-violating [54,55] topological term that can be written as [56]

$$\Delta \mathcal{L} = \epsilon^{\mu\nu\sigma\lambda} \frac{\theta}{64\pi^2} \mathcal{F}_{\mu\nu}^a \mathcal{F}_{\sigma\lambda}^a, \quad (39)$$

where θ is the QCD vacuum angle and $\mathcal{F}^a$ stands for the gluonic field strength tensor. For direct comparison to lattice measurements, we follow the conventions where g is absorbed in the definition of $\mathcal{F}$.

An important quantity is the topological susceptibility [57] as a function of T,

$$\chi_t = \int d^4 x \langle Q_t(x) Q_t(0) \rangle, \quad (40)$$

where

$$Q_t(x) = -\epsilon^{\mu\nu\sigma\lambda} \frac{1}{64\pi^2} \mathcal{F}_{\mu\nu}^a \mathcal{F}_{\sigma\lambda}^a. \quad (41)$$

It can be related to the thermodynamic derivative of the free energy [58],

$$\left. \frac{d^2 \Omega}{d\theta^2} \right|_{a=0} = \chi_t. \quad (42)$$

One reason why χ_t is important is that in QCD, χ_t can be formally related to the mass of the axion field [59,60]. The existence of a dynamical axion is considered to be a possible solution to the strong CP problem (the absence of charge and parity violation in strong interaction) [59]. θ can be related to the QCD axion field (a) via the relation $\theta = a/f_a$, with f_a being the axion decay constant.

It is also well known [61] that this term [Eq. (39)] can be removed by making a $U(1)_A$ transformation on the fermionic field,

$$\psi \to e^{-i\gamma^5 \theta/4} \psi, \qquad \bar{\psi} \to \bar{\psi} e^{-i\gamma^5 \theta/4}. \quad (43)$$

Using the fact that the fermionic measure of the gauge theory is not invariant under the chiral transformations, it was shown that $\Delta \mathcal{L}$ [Eq. (39)] cancels out. Now, under the above mentioned chiral transformation, both the Lagrangian (5) and the mass term are not invariant and pick up a phase factor. θ then appears in the fermionic sector.

For the calculation of χ_t in effective models without dynamic gluonic degrees of freedom, it is assumed that the same procedure follows [62–64]. Namely, θ can be introduced in the fermionic sector using Eq. (43).

Under Eq. (43) the currents transform as

$$j_a(x)/\tilde{j}_a(x) \to \int d^4 z \mathcal{H}(z) \bar{\psi} \left(x + \frac{z}{2} \right) e^{-i\gamma_5 \theta} \Gamma_a / \tilde{\Gamma}_a \psi \left(x - \frac{z}{2} \right). \quad (44)$$

It is clear that the transformations [Eq. (44)] are the same as those for local currents. This is because the $U(1)_A$ transformations that we are making are global.

Therefore, $\mathcal{L}_1$ remains unchanged after going through the transformations Eq. (44), but $\mathcal{L}_2$ transforms to

$$\mathcal{L}_2 \to \mathcal{L}_a = G_2[\cos\theta\{j_a(x)j_a(x) - \tilde{j}_a(x)\tilde{j}_a(x)\} + 2\sin\theta\{j_0(x)\tilde{j}_0(x) - j_i(x)\tilde{j}_i(x)\}], \quad (45)$$

where i runs from 1 to 3. It can be easily verified that the Lagrangian in Eq. (45) is chirally symmetric but breaks the $U(1)_A$ symmetry as required by QCD. Now with the inclusion of the axion field the new working Lagrangian becomes

$$\mathcal{L}_{\text{NJL}} = \mathcal{L}_0 + \mathcal{L}_1 + \mathcal{L}_a. \quad (46)$$

There is also an additional change in the mass term [Eq. (3)], but this additional contribution is small because of the smallness of m. Therefore, we ignore the explicit breaking of $U(1)_A$ by the mass term and consider only contributions from Eq. (5).

Once we have the total Lagrangian, we can get the thermodynamic potential (Ω) using the mean field approximation [51,52,62,63]. To make the above Lagrangian bilinear in quark fields, we follow the same procedure used in the previous subsection. As nonzero θ breaks P, T, and CP symmetry, we can have nonzero mean fields associated with the axial currents. Thus, with the mean-fields σ_s, π_s^3 we now, as well, consider the parity violating mean-fields σ_{ps} and π_{ps}^3. The topological susceptibility is calculated from Eq. (42) at $\theta = 0$, which makes the newly introduced fields go to zero. The quark contribution to the free energy looks the same as obtained in the previous subsection with modifications in the mass term as given below,

$$M^{\lambda,f}_{q_\parallel,k} = M^{\lambda,f}_{0,q_\parallel,k} + s_f M^{\lambda,f}_{3,q_\parallel,k},$$

$$M^{\lambda,f}_{0,q_\parallel,k} = m + A^{\lambda,f}_{q_\parallel,k}\{A\sigma_s + D\sigma_{ps} + (C\sigma_s + B\sigma_{ps})i\gamma_5\} \quad \text{and}$$

$$M^{\lambda,f}_{3,q_\parallel,k} = A^{\lambda,f}_{q_\parallel,k}\{B\pi^3_s - C\pi^3_{ps} + (A\pi^3_{ps} - D\pi^3_s)i\gamma_5\}. \tag{47}$$

Here, $A = (1 - 2c\sin^2(\theta/2))$, $B = (1 - 2c\cos^2(\theta/2))/(1-2c)$, $C = c\sin(\theta)$, and $D = c\sin(\theta)/(1-2c)$. In absence of an axion field (i.e., at $\theta = 0$), we have $A = B = 1$ and $C = D = 0$, which then lead us to the expression obtained in the previous subsection. The eigenvalues are straightforward to calculate. The pure mean field contribution to the free energy is given below,

$$\Omega_{MF} = \frac{A}{2G_0}(\sigma_s^2 + (\pi^3_{ps})^2) + \frac{B}{2(1-2c)G_0}(\sigma_{ps}^2 + (\pi^3_s)^2)$$
$$+ \frac{C}{(1-2c)G_0}(\sigma_s\sigma_{ps} - \pi^3_s\pi^3_{ps}). \tag{48}$$

With these modifications, one can write down the free energy which looks like Eq. (29) with the modified mass eigenvalues and the mean field part replaced by the above expression [Eq. (48)]. With this free energy, we have four gap equations associated with four meanfields. Now from Ω, one can obtain different mean fields by solving the gap equations simultaneously. But as the topological susceptibility is calculated at $\theta = 0$, which forces σ_{ps} and π^3_{ps} to acquire zero values. Hence, the free energy is the same as what we obtained by considering only two mean fields. But to calculate the topological susceptibility, we need the second derivatives of the free energy with respect to all the mean fields and then set σ_{ps} and π^3_{ps} to zero. For specific temperature and magnetic field, these solutions will also depend on θ and thus as a whole, the potential will be

$$\Omega = \Omega(T, eB, \theta). \tag{49}$$

The total derivative of the free energy with respect to θ can be expressed in terms of the partial derivatives of the same with respect to the mean fields and θ,

$$\frac{d^2\Omega}{d\theta^2} = \frac{\partial^2\Omega}{\partial\theta^2} + 2\frac{\partial^2\Omega}{\partial\pi^3_{ps}\partial\theta}\frac{\partial\pi^3_{ps}}{\partial\theta} + \frac{\partial^2\Omega}{\partial\pi^{3\,2}_{ps}}\left(\frac{\partial\pi^3_{ps}}{\partial\theta}\right)^2 + 2\frac{\partial^2\Omega}{\partial\pi^3_s\partial\theta}\frac{\partial\pi^3_s}{\partial\theta} + 2\frac{\partial^2\Omega}{\partial\pi^3_s\partial\pi^3_{ps}}\frac{\partial\pi^3_s}{\partial\theta}\frac{\partial\pi^3_{ps}}{\partial\theta} + \frac{\partial^2\Omega}{\partial\pi^{3\,2}_s}\left(\frac{\partial\pi^3_s}{\partial\theta}\right)^2$$
$$+ 2\frac{\partial^2\Omega}{\partial\sigma_{ps}\partial\theta}\frac{\partial\sigma_{ps}}{\partial\theta} + 2\frac{\partial^2\Omega}{\partial\sigma_{ps}\partial\pi^3_{ps}}\frac{\partial\sigma_{ps}}{\partial\theta}\frac{\partial\pi^3_{ps}}{\partial\theta} + 2\frac{\partial^2\Omega}{\partial\sigma_{ps}\partial\pi^3_s}\frac{\partial\sigma_{ps}}{\partial\theta}\frac{\partial\pi^3_s}{\partial\theta} + \frac{\partial^2\Omega}{\partial\sigma_{ps}^2}\left(\frac{\partial\sigma_{ps}}{\partial\theta}\right)^2 + 2\frac{\partial^2\Omega}{\partial\sigma_s\partial\theta}\frac{\partial\sigma_s}{\partial\theta}$$
$$+ 2\frac{\partial^2\Omega}{\partial\sigma_s\partial\pi^3_{ps}}\frac{\partial\sigma_s}{\partial\theta}\frac{\partial\pi^3_{ps}}{\partial\theta} + 2\frac{\partial^2\Omega}{\partial\sigma_s\partial\pi^3_s}\frac{\partial\sigma_s}{\partial\theta}\frac{\partial\pi^3_s}{\partial\theta} + 2\frac{\partial^2\Omega}{\partial\sigma_s\partial\sigma_{ps}}\frac{\partial\sigma_s}{\partial\theta}\frac{\partial\sigma_{ps}}{\partial\theta} + \frac{\partial^2\Omega}{\partial\sigma_s^2}\left(\frac{\partial\sigma_s}{\partial\theta}\right)^2 + \frac{\partial\Omega}{\partial\sigma_s}\frac{\partial^2\sigma_s}{\partial\theta^2}$$
$$+ \frac{\partial\Omega}{\partial\pi^3_s}\frac{\partial^2\pi^3_s}{\partial\theta^2} + \frac{\partial\Omega}{\partial\sigma_{ps}}\frac{\partial^2\sigma_{ps}}{\partial\theta^2} + \frac{\partial\Omega}{\partial\pi^3_{ps}}\frac{\partial^2\pi^3_{ps}}{\partial\theta^2}. \tag{50}$$

Each of the last four terms contains gap equations, which are zero at the minima of the free energy. Using the above expression, we can now calculate χ_t from Eq. (42). For a recent calculation of χ_t in the local NJL model with $eB = 0$, see [51], and for nonzero eB, see [52].

III. RESULTS

A. Choice of the fitting observables for $eB = 0$ and the ranges of parameters

As discussed above, the nonlocal NJL model for $eB = 0$ has three parameters G_0, Λ, and m. (c plays a role only for $eB \neq 0$.) To fix these, we would like to fit the model to match three independent observables. In this paper, we will work only with the two-flavor model. We fit the three parameters to self-consistently determined data from (two-flavor) lattice calculations for m_π, F_π and $\langle\bar{\psi}_f\psi_f\rangle$ in the absence of a magnetic field. With this parameter set, we study the behavior of u and d condensates in the presence of magnetic field within the nonlocal NJL model and

compare them with the lattice results of Ref. [16] for zero as well as nonzero temperatures.

The lattice study in Ref. [16] is done for physical pions, and they also quote the value of F_π in the chiral limit (86 MeV). However, since the value of the condensate for this lattice calculation was not available in the literature, we use other lattice calculations to fit the parameters of our model.

We do note that the results of Ref. [16] are for $1 + 1 + 1$ QCD, and hence, the model fitted to two flavor data cannot be expected to capture the physics of the three flavor model completely. Indeed, as we will see below, the crossover temperature for $eB = 0$ we obtain is lower than the crossover temperature in Ref. [16]. This is a well-known property of the nonlocal NJL model [33]. A direct comparison will require the generalization of the model to three flavors, which we will consider in future work. However, here, we study to what extent the two flavor model captures the results found in Ref. [16] and hope that once the temperature is scaled by the scale T_{CO}, the dependence on the flavor content is not very strong.
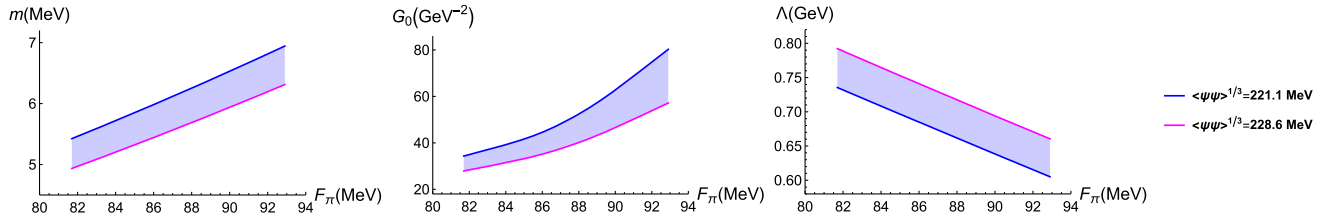
FIG. 1. Range of model parameters to access the full allowed range of the condensate, including the errors as given in LQCD [48] (JLQCD).

To cover a range of self-consistently determined parameter values, we consider a two-flavor LQCD calculation to constrain our model [48] (referred in the text as JLQCD), which we discuss in detail in the following sections. We also consider another LQCD data set [49] (we refer to it as Brandt13), for which the analysis is briefly discussed in the Appendix. One can look into the Ref. [47] for the available lattice results and the latest developments. The calculation in [48] is performed at the physical m_π and the error on m_π is assumed to be negligible. We fit to F_π at the physical pion mass.

We begin our search for finding parameter space for the model with the JLQCD data set. The condensate and the decay constant (with the error estimates) are given in Ref. [47], and we quote them below,

$$\langle \bar{\psi}\psi \rangle^{1/3}|_{\mu=2 \text{ GeV}} = 240(4) \text{ MeV} \quad \text{and}$$
$$F_\pi = 87.3(5.6) \text{ MeV}. \qquad (51)$$

One should note that the quoted value of the condensate from the LQCD study has been obtained at the renormalization scale $\mu = 2$ GeV [48]. A direct matching of this value to the effective models is difficult because of two reasons. First, the natural scale for the kind of effective models that we are considering here is around 1 GeV (for the nonlocal model, Λ provides a rough estimate of the cutoff, which is ~ 1 GeV; see Figs. 1 and 2). Second, the renormalization scheme in the effective models is usually not $\overline{\text{MS}}$.

The correction due to a difference in schemes is a systematic that we can not presently correct. However, we can consider the effect of the difference in the energy scales by renormalization group (RG) techniques. In order to express the LQCD results at the scales suitable for the

model, we exploit the perturbative renormalization group running for the condensate calculated in [65–67]. This has been previously used for example in Ref. [68]. We estimate the condensate value at $\mu = 1$ GeV and found it to be

$$\langle \bar{\psi}\psi \rangle^{1/3}|_{\mu=1 \text{ GeV}} = 224.8(3.7) \text{ MeV}. \qquad (52)$$

On the other hand, F_π being a scale-independent quantity remains unchanged.

With m_π fixed to its physical value 135 MeV, we explore the allowed region for the parameters by considering the central value of F_π and its $\pm 1\sigma$ variation, and similarly for the condensate. Thus, we obtain a total of nine parameter sets to cover the allowed range provided by the quoted data.

Reference [43] considered condensates in the range $\langle \bar{\psi}_f \psi_f \rangle^{1/3} = 210$–240 MeV and showed that the appearance of IMC in the crossover region in the nonlocal NJL model depends on the values of the condensates. They showed that for condensates larger than 240 MeV, T_{CO} increases as one increases eB for smaller eB (for the Gaussian form factor), in contradiction with lattice observations. The motivation for the considered range of the condensate in Ref. [43], comes from the cited articles [69,70]. One of them [69], using chiral perturbation theory, calculated the condensate to be in the range $(200$–260 MeV$)^3$ and the other article [70], from a model calculation with fermions interacting via instanton-induced interaction, deduces the condensate to be $(270 \text{ MeV})^3$. However, the value of F_π was fixed to be the physical value. With the more controlled lattice results now available on F_π and the condensate, one of the motivations for our paper is to fit the model to these. We find that IMC near T_{CO}, sensitively, also depends on the value of F_π.
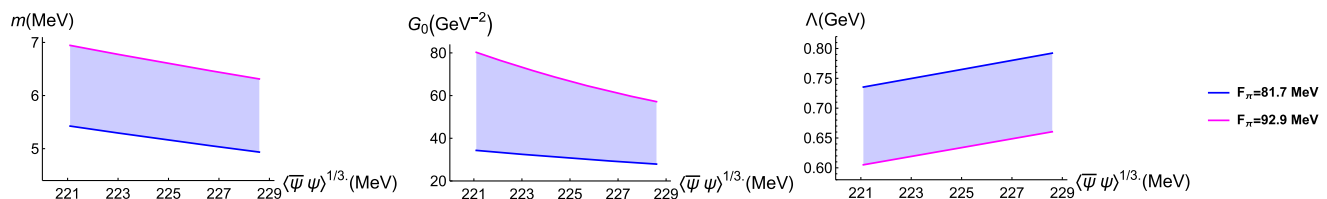

FIG. 2. Range of model parameters to access the full allowed range of the pion decay constant (PDC), including the errors as given in LQCD [48] (JLQCD).

TABLE I. Central and the four corner parameter sets associated with the Figs. 1 and 2 for LQCD data [48]. The quantities in the last four columns pertain to the nonlocal NJL model. The values of the condensate are at $\mu = 1$ GeV, obtained following perturbation RG running used in the Ref. [68].

	$\langle \overline{\psi_f} \psi_f \rangle^{1/3}$ (MeV)	m_π (MeV)	F_π (MeV)	$F_{\pi,0}$ (MeV)	m (MeV)	G_0 (GeV^{-2})	Λ (MeV)
Parameter set CC	224.8	135	87.3	84.25	5.87	43.34	697.22
Parameter set HH	228.6	135	92.9	90.63	6.31	57.15	660.46
Parameter set HL	228.6	135	81.7	77.04	4.94	27.90	792.22
Parameter set LH	221.1	135	92.9	91.00	6.94	80.26	605.05
Parameter set LL	221.1	135	81.7	77.61	5.42	34.32	735.38

Figures 1 and 2 represent the range of the model parameters as allowed by the JLQCD observables in the form of bands. These bands are drawn using the nine parameter sets that we have, including the errors. In Fig. 1, the bands are obtained for different condensate values as a function of F_π. On the other hand, they are shown for different F_π's as a function of condensate in Fig. 2. The upper and lower lines of the bands are for two extreme sets of observables ($\langle \bar{\psi}\psi \rangle^{1/3}, F_\pi$)—the blue and the magenta lines are for lowest and highest values, respectively. It is further to be noted from Fig. 1, that as we increase F_π for a given value of condensate the parameter Λ decreases whereas G_0 increases. On the other hand, in Fig. 2, it is the other way around, i.e., as the condensate is increased Λ increases and G_0 decreases, for a given value of F_π. Now Λ controls how the effective coupling runs as a function of momentum, i.e., how fast the effective coupling decreases with momentum. This information will be helpful in qualitatively understanding the results for finite eB from different parameter sets. Out of these nine parameter sets, we will investigate in detail only five—the central value along with the four corners.

In Table I, for further illustration, we have presented the central parameter set and the four corner parameter sets associated with Figs. 1 and 2. The letters C, H, and L stand for central, highest, and lowest values, respectively. The first letter corresponds to the value of condensate and the second one to the value of F_π. These are the five parameter sets from JLQCD that we work with. Just to remind our readers, we mention here again that the condensate values shown in the second column of the Table I are calculated at $\mu = 1$ GeV by using the perturbation RG running [68], and the values are roughly 15 MeV smaller than their corresponding LQCD values estimated at $\mu = 2$ GeV.

In the scaled definition of the condensate given by Eq. (38), we need to use F_π in the chiral limit (denoted as $F_{\pi,0}$). In Fig. 3, we present the chiral limit behavior of the F_π and the condensate in the model by keeping G_0 and Λ fixed and only changing m to 0. This is a self-consistent way to obtain the chiral limit within the model.

To give more details about the chiral extrapolation, in the left panel of Fig. 3, we show the plot of F_π for the central value of condensate (224.8 MeV) and in the right panel, the plot for condensate, for three different values of F_π (L, C and H) as allowed by the JLQCD observables. One should necessarily note here that the mentioned values for the condensate and F_π (CC, CL and CH) are to be interpreted only for the fitted values of current quark mass (m), because eventually in both the plots, neither of them is constant as a function of m. We learn from there that as we increase the pion mass, F_π increases with an almost constant slope. On the other hand, the condensate also increases with the pion mass but the slope depends on the values of F_π—it decreases as the value of F_π is increased.

In the next subsection, we describe the parameter fitting at zero temperature but nonzero magnetic field.

B. Magnetic field dependence at zero temperature

In this subsection, we fit the explicit $U(1)_A$ symmetry breaking parameter (c) with the LQCD data [16] at zero
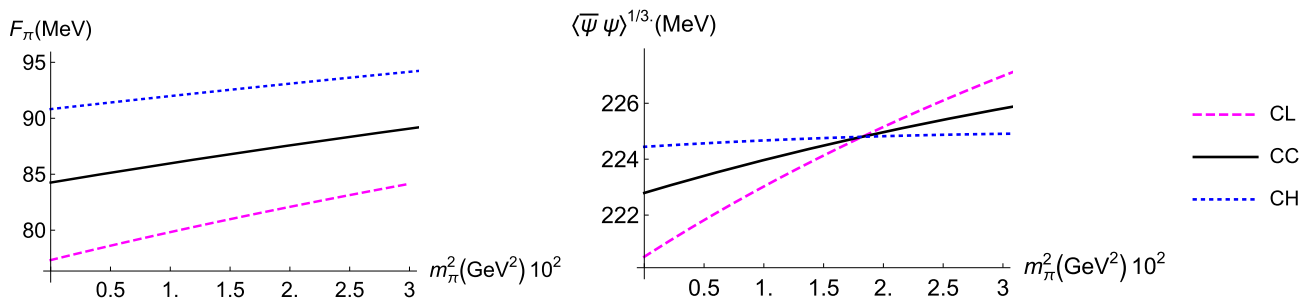

FIG. 3. Pion decay constant and condensate in the chiral limit with G_0 and Λ kept fixed. The left panel is obtained for the central value of condensate (224.8 MeV), whereas for the right panel plot, three different values of F_π have been used (see Table I).

T and nonzero eB. The lattice simulation provides us with the average and difference of the condensates. In the model calculation, the condensate average is independent of c, but the difference depends on it. So we use the values of condensate differences to fit c at zero T and nonzero eB. Then we further use this fitted value to predict the nonzero T and eB behavior of the condensate in the model and compare them with the lattice data in the next subsection.

First, let us consider the condensate average. Analyzing the JLQCD set, we compare the model results with the LQCD data in Fig. 4, using their normalized definition of condensate as given in Eq. (38). It shows that for the CC parameter set the matching with the LQCD data is very good even for finite eB. Black points are used to denote the CC parameter and LQCD data are shown with the red points. Using the corner parameter sets, we obtain the spread in average condensate, which is also shown with the dashed blue (HL) and green (LH) lines. For $eB = 0$, the curves meet at unity just from the definition [Eq. (38)].

What is interesting is that for the central value (CC) of the parameters, the condensate average agrees very well with results from Ref. [16]. (The black points completely overlap with the red points within error bars.) However, for the corners of the parameter space (LL, LH, HL, and HH), the agreement with the lattice results is not as good: the slope for the eB variation does not match LQCD. We examine this more carefully below.

In Ref. [33], it was already shown that the scaled condensate given by Eq. (38) has a mild dependence on the actual value of condensate and F_π was kept fixed. Here, we have explored the F_π dependence on all observable quantities and as there is a significant difference in F_π, hence in $F_{\pi,0}$ for the corner parameter sets, we obtain a spread in the (scaled) average condensate.

The implication for the comparison in Fig. 4 is that the normalization factor $\mathcal{N}^2 = (m_\pi F_{\pi,0})^2$ is very sensitive to $F_{\pi,0}$ and hence, gives rise to the different slopes: the larger values of $F_{\pi,0}$ lead to a smaller slope and vice versa. In the lattice calculation in Ref. [16], $F_{\pi,0}$ is taken to be 86 MeV. Figure 4 shows the range of average condensate we obtain
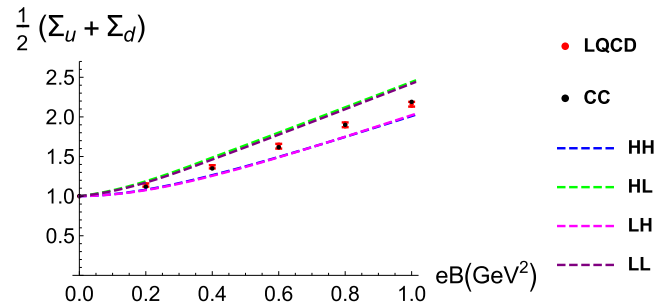
TABLE II. χ^2 fitting of condensate difference in c for all the five parameter sets from JLQCD.

	c	χ^2 per d.o.f.
Parameter set CC	0.276 ± 0.068	0.211
Parameter set HH	0.044 ± 0.079	0.149
Parameter set HL	0.374 ± 0.051	0.290
Parameter set LH	0.149 ± 0.103	0.634
Parameter set LL	0.465 ± 0.062	0.551

when we vary $F_{\pi,0}$ in the range of values self-consistently determined with the condensate.

Now we analyze the effect of c. First, we keep $eB = 0$ and think about constraints on c due to general physical considerations. As mentioned above, F_π, m_π, and the condensate average are independent of c. $\Sigma_u - \Sigma_d = 0$ for $eB = 0$ irrespective of the value of c. But certain fluctuations are sensitive to the value of c even for $eB = 0$. More specifically, the mass of the fluctuations in the isoscalar pseudoscalar channel [71] depends on c. In the two flavor problem, this is often called η^* [71] and can be intuitively thought of as a fictitious mixture of η and η' mesons present in the full three-flavor theory. Since there is no physical particle directly corresponding to the η^*, the meson spectrum in the two flavor theory can not be directly used to find c. However, physical considerations do restrict the allowed values of c in the theory.

At $c = 0$, η^* becomes degenerate with π^0. This is a simple consequence of the restoration of the $U(1)_A$ symmetry in this limit. On the other hand, considering η^* as a mixture of η and η' one would expect the mass of η^* to be a few times to that of π^0. This sets a lower bound on the value of c. To be precise, we impose the physically motivated constraint that $M_{\eta^*} > 400$ MeV.[1] In Fig. 11 (in Appendix A), we have shown the M_{η^*}, obtained using the expression from Ref. [72], as a function of c for the CC parameter set and the assumed constraint on M_{η^*} allows c to be greater than 0.12. This should be mentioned here that changing the parameter set will have a negligible effect on the constraint. This gives $c > 0.12$. At the other end, η^* becomes tachyonic for $c > 1/2$. Therefore, these physical constraints restrict, c to be in the following region:

$$c \in [0.12, 0.5]. \tag{53}$$

Below we first consider the effect of c on condensate difference for finite eB without imposing the physically motivated constraints on c [Eq. (53)]. These results are given in Table II.

---

[1]We should remind ourselves that this limit is not of a very strict nature because of the flavor number we are considering here. But we will eventually find out that the kind of c limit that this approximated value of M_{η^*} provides us is reasonable for having the appropriate strength of topological susceptibility and is also comparable with other known studies.
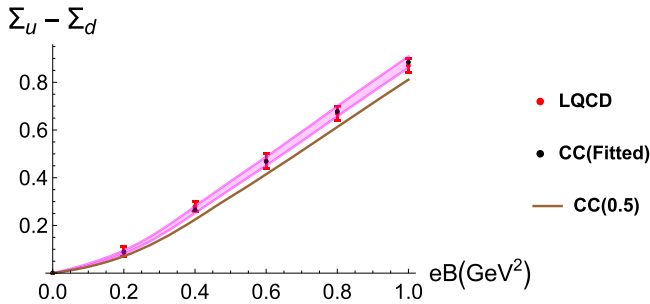

$\frac{1}{2}(\Sigma_u + \Sigma_d)$

FIG. 4. The condensate average as function of magnetic field as compared with LQCD [16] data for JLQCD.

FIG. 5.   The condensate differences (u and d) fitted in c for parameter set CC in JLQCD for LQCD data [16].

For finite eB, $\Sigma_u - \Sigma_d$ grows as eB increases, and the rate of this increase is sensitive to c, and we use this dependence to fit c.

As an illustrative example, in Fig. 5, we show the best fit for the CC parameters along with the uncertainty in c. In principle, there is no reason why c cannot depend on eB, but we see from the same figure that a one-parameter fit in c is quite adequate to describe the data. It is drawn with the fitted value of c along with its uncertainty shown as a magenta coloured band. We see from Table II, where the $\chi^2/\mathrm{d.o.f.}$ is shown, $c = 0.276 \pm 0.068$ describes the data well for CC. The conclusion is that the data for $\Sigma_u - \Sigma_d$ as a function of eB allow us to extract the value of c, which can then be used to compute additional observables (for example, topological susceptibility) everywhere through the range from $eB = 0$ to about 1 GeV^2.

In the pursuit of narrowing down further to find the best possible parameter set for the model, we look at the fitted c values from Table II.

The fittings for the other four corner parameter sets are summarized in Table II, which contains both the fitted c values along with their uncertainty and the corresponding $\chi^2/\mathrm{d.o.f.}$. We see that the quality of fits in c is quite satisfactory. We would like to mention here that the parameter c can be constrained further with reduced errors, once we have better-controlled LQCD data with narrower error bands for the $\Sigma_u - \Sigma_d$.

Now with these fitted c values we will explore the nonzero T behaviour of both the condensate average and the difference.

C. Results for nonzero temperature

1. Condensate average and the phase diagram

In this subsection, we study the results for condensate average at both nonzero T and eB. The main assumption here is that the parameters G_0, Λ, m, and c are independent of eB and T, and we use the values fitted at $T = 0$ for all of these (Tables I and II) and compare the results with the LQCD data [16]. The value of the average condensate is very insensitive to c if we vary it within the range [0, 1]. Though we mention here the full range of c as from 0 to 1,

but for our analysis we never go beyond $c = 1/2$ and the reason for this along with the implications have been mentioned in detail in the previous subsection before Eq. (53) and also in the next subsection after Eq. (55). In principle, we can start the discussion in this section from any parameter set from Table I, and we design our analysis in the following manner. First, we explore all the five available parameter sets and look for the ones for which the IMC effect is obtained satisfactorily as compared to the LQCD data [16]. This part of the analysis is almost independent of the values of c and will leave us with a fewer number of parameter sets. then we see the effect of c.

Following the preceding argument, initially, we have two parameter sets to deal with—one is the LH parameter set (221.1,92.9) and the other is the HH (228.6,92.9) one, both of which reproduce the IMC effect reasonably well (Fig. 7) as compared to the LQCD data [16]. Then we refer back to the fitted c values (Table II) for these two parameter sets and chose LH (0.149 ± 0.103) over HH (0.044 ± 0.079) by the following arguments. Further imposing the physical constraint in Eq. (53) eliminates the allowed region for HH, and hence, from now on, we focus on the LH data set only. The allowed c value for LH parameter set, after taking into consideration the constraint, becomes

$$c = 0.149^{+0.103}_{-0.029}. \tag{54}$$

As we have argued that the LH parameter set is the best possible parameter set in the model, we display the plot of the temperature dependence of average condensate in Fig. 6 for the corresponding parameter set. In the figure, we have used five different values of eB, the top left panel is for 0.2 GeV^2, and we increase eB in steps of 0.2 GeV^2 from left to right. We observe that the results from the model (Fig. 6) agree reasonably well with the LQCD data.

The crossover temperatures from the LQCD calculation [16] for $eB = 0$ and in the present model are different. For a clear notation, we call this T_{CO}. The crossover temperature at finite eB we will call $T_{CO}(eB)$. The value of T_{CO} in Ref. [16] is given to be 158 MeV. The values for the model are shown in Table III. The crossover temperature in both is defined as the inflection point of the average condensate.

It is to be noted here that the overall scale of the thermal transition is not captured in the model, as the predicted critical temperatures (Table III) are found to be relatively low as compared to the known standard LQCD results. This is usually the case with the nonlocal NJL model [33]. This can be improved with the standard technique of including Polyakov loop (PL) [32]. In spite of an underprediction of the transition temperature in the model, to see if the model describes how the condensate changes as a function of the ratio of the temperature to the crossover scale, we follow previous literature and compare our calculations with lattice calculations as a function of T/T_{CO}. We keep the inclusion of PL for the future endeavour, particularly it will be really
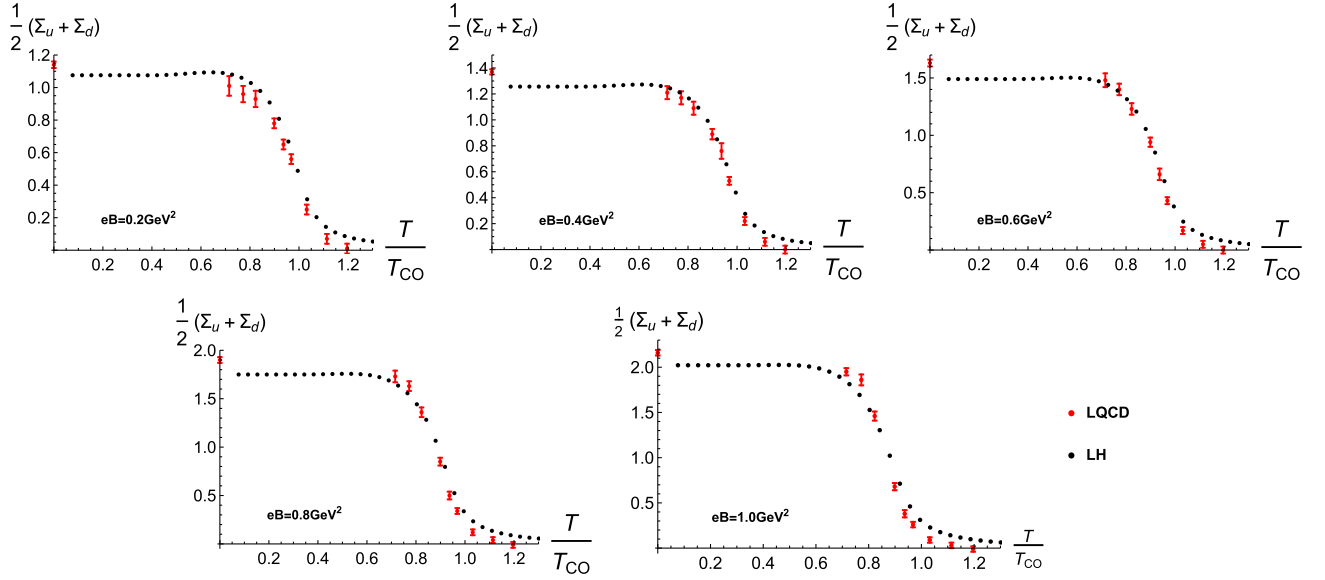
FIG. 6.   Plot of condensate average for different values of magnetic field as a function of temperature for parameter set LH of JLQCD, along with the comparison with LQCD data [16].

interesting to observe the behavior of the $U(1)_A$ symmetry breaking parameter c in the presence of background gauge field.

It is expected from the figure above that the crossover temperature in the model for the LH parameter set will be very close to that of LQCD as eB is increased. This is what is observed from Fig. 7, where the predicted phase diagrams for all five parameter sets are displayed. As already mentioned, it is noted from the phase diagram that the decrease of $T_{CO}(eB)$ as a function of the magnetic field as obtained in LQCD simulation is not satisfactorily reproduced with all the parameter sets. HL (228.6,81.7) and LL (221.1,81.7) parameter sets fail to produce the IMC effect. Though the CC (224.8,87.3) parameter set can reproduce the IMC effect, it is not very satisfactory as compared to LQCD data. Only for the LH and HH parameter sets we see a comparable reproduction of the IMC effect.

From the phase diagram, we find this important message that we get a better agreement with LQCD results as we decrease the condensate and/or increase F_π. The necessity of smaller values of the condensate has already been demonstrated by Scoccola *et al.* (see the left panel of Fig. 3 in Ref. [33] for the Gaussian form factor). But our analysis indicates that whether the nonlocal effective QCD
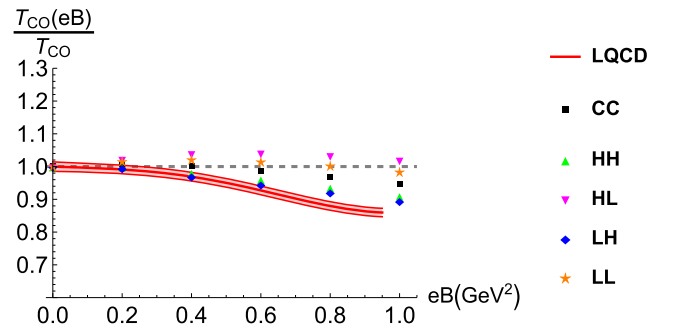

FIG. 7.   The phase diagram in $T - eB$ plane for parameter sets obtained to reproduce JLQCD vacuum observables, compared with that from LQCD study [15].

model shows the IMC effect also depends on the values of F_π. This observation becomes apparent when the analysis is performed with sets of self-consistent parameters fitted to LQCD results.[2] This observation in the effective model scenarios, to the extent of our knowledge, has not been reported before.

As discussed in Sec. III A, this observation can be related to the constants of the model, namely Λ and the coupling constant (G_0). We observe that lower Λ and higher G_0 gives a better agreement with LQCD results. One of the important features of the nonlocal NJL model is that it captures an important property of QCD, the running of coupling constant, which gives rise to the asymptotic freedom. For higher Λ, the effective coupling constant decreases

TABLE III.   Crossover temperature at $eB = 0$ (we call this T_{CO}) for all parameter sets of JLQCD in MeV.

Parameter set	CC	HH	HL	LH	LL
JLQCD	122.282	130.156	115.577	130.664	115.041

---

[2]We find that there is a difference in the value of m_π between Ref. [33] and us. Their quoted value is 139 MeV.
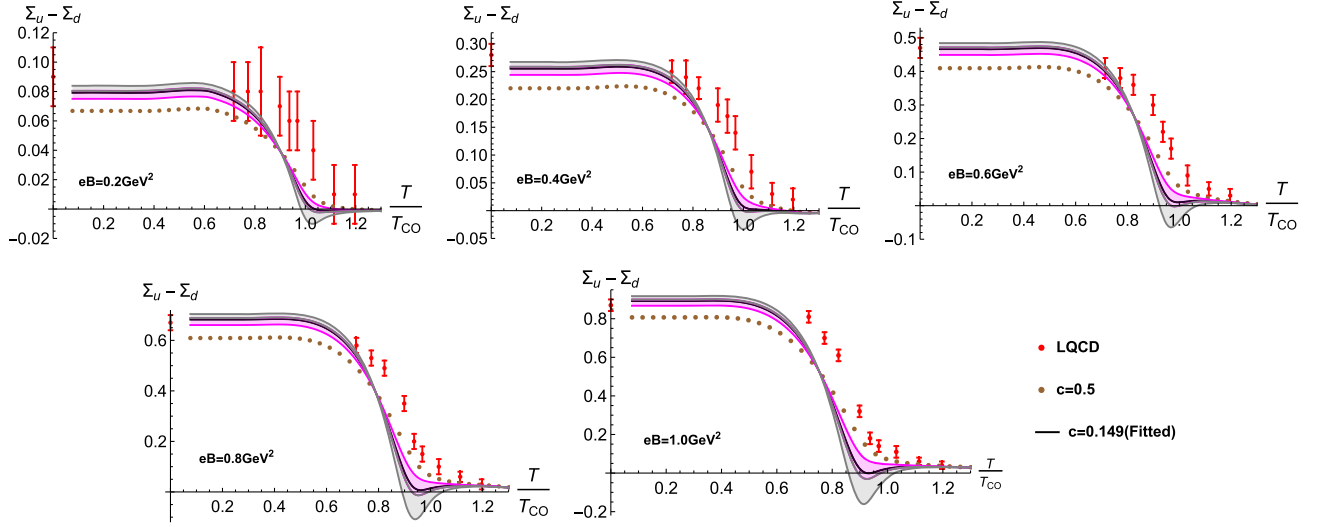
FIG. 8. Plot of condensate difference for different values of magnetic field as a function of temperature for parameter set LH of JLQCD.

with a slower rate as compared to smaller Λ and thus, getting more contribution from higher momentum modes. It leads to delay in achieving asymptotic freedom, which is crucial for obtaining IMC effect [21,22,73].

2. Condensate difference

In this subsection, we describe the condensate difference obtained by using the same LH parameter sets and compare them with the LQCD findings for different strengths of eB.

To understand the results it is helpful to review the idea of "flavor mixing" [44] in the presence of backgrounds that break isospin symmetry. The idea is most cleanly displayed for the local NJL model, where the constituent masses [the analog of Eq. (28)] are given by

$$M_u = m - 4G_1\langle \bar{u}u \rangle - 4G_2\langle \bar{d}d \rangle$$
$$M_d = m - 4G_1\langle \bar{d}d \rangle - 4G_2\langle \bar{u}u \rangle, \qquad (55)$$

where G_1, G_2 are given in Eq. (7). In particular, for $c = 0$, $G_2 = 0$ and M_u decouples from $\langle \bar{d}d \rangle$ and vice versa, and the equations for the two condensates are independent. For $c = 1$, $G_1 = 0$ and the gap equations for the two condensates are maximally coupled. In terms of the Lagrangian, $c = 0$ implies $\mathcal{L}_2$ [Eq. (5)] is set to zero, which further signifies complete flavor decoupling and maximal "flavor mixing" corresponds to $c = 1$, which implies that $\mathcal{L}_1$ [Eq. (4)] is set to zero. For the nonlocal model, the relation between $\sigma_s + \pi_s$ ($\sigma_s - \pi_s$) and $\langle \bar{u}u \rangle$ ($\langle \bar{d}d \rangle$) is more complicated, but the intuition that the two gap equations decouple for $c = 0$ still holds. In our analysis, we explore only up to the $c = 1/2$ as the reference point, since beyond that 't Hooft mass becomes imaginary; i.e., η^* becomes a tachyon [71].

With these intuitions in mind, we show the Fig. 8 displaying the plot for the condensate difference for the LH parameter set for different values of eB. The band shows the uncertainty in the fitted c value.

More concretely, the uncertainty marked in the figure by a gray band corresponds to the fitted value 0.149 ± 0.103 at $T = 0$ (Table II). Further imposing the condition $c > 0.12$ (Sec. III B), a part of the gray band (from $c = 0.046$ to 0.12) gets excluded, and the magenta band remains as a prediction from the model as given by our final fitted c value ($0.149^{+0.103}_{-0.029}$) in Eq. (54). In the figure, we have also shown the behavior for $c = 1/2$ as a reference line; at that value of c, the model reduces back to the usual NJL model. This figure sheds some light on how the "flavor mixing" effects impact the behavior of condensate difference in presence of eB at finite T. We note that the condensate difference calculated in the model matches well with the LQCD data up to the temperature $0.8 T/T_{CO}$, and then it falls at a bit faster rate than the LQCD data.

One interesting thing to notice in Fig. 8 is that around the crossover temperature, for a part of the gray band corresponding to the lowest c values, the condensate difference ($\Sigma_u - \Sigma_d$) becomes negative and then increases and gradually merges with the LQCD data at higher values of T. It is quite heartening that for the magenta band for which the lowest values of c are excluded based on physical arguments, this peculiar behavior is clipped, and the results track closer to lattice results. This oscillatory behavior about $\Sigma_u - \Sigma_d = 0$ at small c in the model can be explained in the following manner.

For any arbitrary strength of the magnetic field at $T = 0$, the u condensate is always greater than the d condensate because its coupling with the magnetic field is twice as strong as that of the d quark. For $c = 0$, as discussed below

Eq. (55), the u and d condensates decouple and can vary independently. For the c values which are small but not 0, the partial decoupling of the u and d condensates leads to an independent drop of Σ_u at a faster rate as T approaches T_{CO} before Σ_d; i.e., the IMC effect is stronger for Σ_u than Σ_d due to a larger $|q_u|$. Hence, $\Sigma_u - \Sigma_d$ becomes negative just before T_{CO}. Eventually, both the condensates catch up and drop asymptotically to 0. At zero magnetic field, $\pi_s = 0$, and c does not have any influence on the condensates. Introduction of a magnetic field separates the two; hence, the stronger the magnetic field greater the effect.

This kind of behavior just below T_{CO} is not a peculiarity of this particular model for small c. In fact, in the local NJL (three flavor) model, a different kind of scenario is also observed, where the d condensate decreases with a faster rate as compared to that of u one resulting in a "bump" like behavior in the condensate difference around the crossover temperature before finally going to zero ([13,22]). The authors explained this using a higher coupling constant of u quark with the magnetic field as compared to d, which relatively delays the decrease of u condensate around the crossover temperature since they consider a constant coupling constant which does not reproduce IMC. This argument is indeed an important way in which such behavior can arise, but as we have found, "flavor mixing" effects could possibly play an important part too.

D. Topological susceptibility

In this section, we describe our model predictions for χ_t. The field a is connected to $U(1)_A$ transformations of the quark field, and hence, the χ_t is related to the extent of the $U(1)_A$ symmetry breaking. $\mathcal{L}_2$ explicitly breaks $U(1)_A$ symmetry. [The small quark mass m also breaks $U(1)_A$ weakly.] Furthermore, the chiral condensate spontaneously breaks $U(1)_A$. Hence, we expect that the topological susceptibility is sensitive to both c and the chiral condensate. In particular, in the chiral limit, if $c = 0$, χ_t will be 0.

We use the fitted c value for LH parameter set (the most suitable parameter set in the present model as established in the previous sections) from Table II to calculate the χ_t using Eq. (42). The plot is shown in Fig. 9 along with two different LQCD results [74,75]. We show the central value of the fitted c, which is 0.149, for three different values of the magnetic field, $eB = 0$, 0.5 and 1.0 GeV^2.

For comparison with the LQCD results, we have used two separate results from LQCD calculations available in the literature. The red band is obtained from the Ref. [74]. In this reference, they used a $2 + 1 + 1$ flavor LQCD and extend their analysis further to give the equation of state in $2 + 1 + 1 + 1$ flavor QCD. But as charm quarks begin to contribute to the equation of state above 300 MeV, they used $2 + 1$ flavors dynamical quarks up to 250 MeV. So this red band used in the Fig. 9 is a $2 + 1$ flavor lattice result for χ_t. In that original paper [74], the authors have given
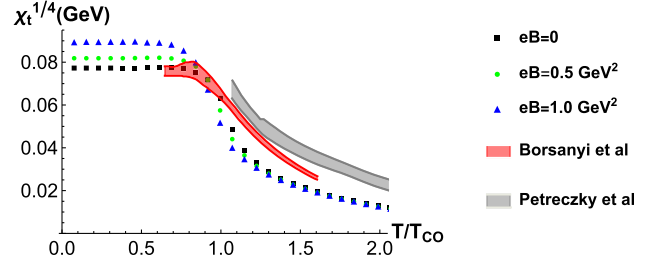

FIG. 9. Topological susceptibility as a function of scaled temperature for the LH parameter set. The red and the gray bands represent lattice results from the Refs. [74,75], respectively.

the plot as a function of temperature. To scale it with the transition temperature, we used Ref. [76], where the authors have given the range of the T_{CO} depending on the observables they use. Since in the model we are calculating the T_{CO} from the inflection point of the condensate, it makes sense that we use the value calculated using the same observable in lattice simulation, which is found to be 155 MeV. There is another LQCD result [75] shown by the gray band, which is also a $2 + 1$ flavor calculation. There the result is already provided as a function of scaled temperature and is given starting from close to T_{CO}.

The black squares in the plot are the model predictions at zero eB with the fitted c value. Below the transition temperature, the model prediction is within the red band given by the only available LQCD data at that range [76]. Although the trend is similar, as the temperature increases further, the model prediction falls at a faster rate. We understand that the model is simple and is deprived of some of the important features of full QCD as that in lattice QCD, but in our opinion, this numerical mismatch could possibly be arising from different flavor number considerations. This hunch can be tested by incorporating another flavor, which is beyond the scope of the present article, and we plan to address it elsewhere.

Then we further explore the impact of the magnetic field on χ_t and learn that it increases with the increase of eB below the transition temperature. This is easily understood as eB increases the condensate at low T. This finding has already been reported in Ref. [52] in the local NJL model. There are two main differences between our calculation and Ref. [52]. The first is that we use a value of c determined by matching to $T = 0$ LQCD results at $T = 0$. Second, we observe that after $1.3T_{CO}$ or so we do not see any effect of magnetic field on χ_t, and they all fall on top of each other, whereas Ref. [52] reported a considerable impact from the magnetic field even after the transition temperature. It is also to be noted from the figure that the IMC effect is well reflected in χ_t around the T_{CO}.

In Fig. 10, we show the sensitivity of the result to the value of c for $eB = 0$. It is drawn for two different values
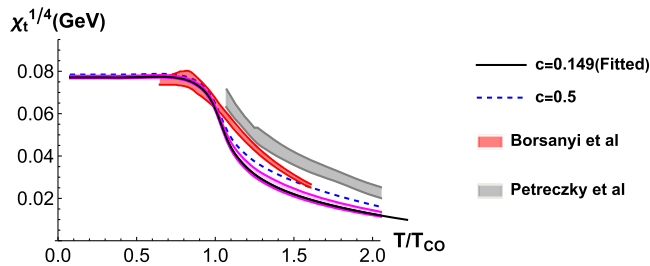
FIG. 10. Topological susceptibility as a function of scaled temperature for different c values for the LH parameter set. The blue dashed line is for $c = 0.5$, and the black solid line is the model prediction with the magenta band representing the uncertainty in c. The red and the gray bands represent lattice results from the Refs. [74,75], respectively.

of c: $c = 0.149$ (the fitted one with solid black line), $c = 1/2$ (standard NJL model with blue dashed line). For the fitted value, we have shown the uncertainty in χ_t as well by the magenta band. This uncertainty arises from the uncertainty in c, given by Eq. (54). At low temperature, the χ_t for these three values are almost the same, and as the temperature is enhanced, they start diverging from one another, particular above the T_{CO}. We see that currently the LQCD results for χ_t cannot distinguish among these values.

IV. CONCLUSIONS AND OUTLOOK

In this paper, we have studied the two flavor nonlocal NJL model in the presence of a magnetic field and explored the chiral crossover. Our investigation builds upon the nonlocal NJL model calculations of Refs. [33,43] with some important additions.

The first is that we add to the nonlocal form of the standard four Fermi NJL interaction, the nonlocal form of the 't Hooft determinant term with an arbitrary coupling constant, which is governed by a dimensionless parameter c. In the Refs. [33,43], c is taken to be $1/2$, which is generally the case in the usual NJL model. In the absence of any isospin symmetry breaking (we assume equal u and d current quark masses), the value of c does not play any role because only the sum of the u and d condensates is nontrivial. But in the presence of isospin symmetry breaking agents like an isospin chemical potential [44] or/and magnetic field [9], the two condensates become different because of their different couplings to the agents. The difference between the u and d condensates is particularly sensitive to c. This is evident from the gap equation associated with π_s^3 [Eq. (31)].

Our second major addition is that we have attempted a more systematic analysis of the parameters of the model by fitting them to a self-consistent set of lattice results. For $eB = 0$, the parameters G_0, Λ, and m were fixed to m_π, F_π, and the condensate (at $T = 0$). We used the lattice result [48] for which we performed the detailed analysis in the

main text. We also use another lattice result [49], the central values of the condensates being different for these two references, and discuss briefly the results of our analysis in the Appendix B.

Then considering $T = 0$ results for finite eB, we found that an eB independent c describes the lattice results for the u, d condensate difference at $T = 0$ quite well, which allows us to extract the value of c using lattice results on the u, d condensate difference. We estimate this observation to be significant, as to our knowledge, for the first time c has been constrained using lattice results.

In the past, efforts have been made to constrain c but from different perspectives than us, particularly by these two Refs. [9,44], which we summarize here to emphasize the difference with our approach. Reference [44] discusses the effect of c on the phase diagram for the small T and high chemical potential (μ) region, in the presence of an isospin chemical potential (μ_I). For zero instanton interactions, the quarks decouple, hence giving rise to different transition lines in the $T - \mu$ plane, though the authors argued that in their respective $T - \mu_I$ plane they will be identical. They obtained a critical value for c above which these two transition lines merge with each other in the $T - \mu$ plane. They also drew an analogy from the three-flavor NJL model to estimate the value of c, which turned out to be close to the one obtained from the phase diagram. Reference [9] has done a similar analysis to Ref. [44] with a nonzero magnetic field instead of an isospin chemical potential. With zero instanton effects, one obtains two different phase transitions. In this paper, they showed that as one introduces the "flavor mixing effects" through c, the transitions come closer to each other, and beyond some critical value of c, they merge to become a single phase transition. In these works, the value of c is found to be approximately within the range of 0.1–0.2.

In our calculation, we analyzed the parameter sets accessible for a given LQCD study and picked the ones which are reproducing the IMC effect suitably as compared to the LQCD result [15]. We found that for the JLQCD data [48] LH (221.1,92.9) and HH (228.6,92.9) parameter sets replicate the IMC effect reasonably well. Further looking at the fitted c values for these two parameter sets, which are 0.149 ± 0.103 and 0.044 ± 0.079, respectively and evoking some basic properties of η^*, we could constrain the plausible range of c. We argued that, as at $c = 0$, η^* becomes degenerate with π^0 and also expecting the mass of η^* to be a few times that of π^0 (considering η^* as a mixture of η and η'), which sets the lower bound in c as $c > 0.12$, thus excluding the HH parameter as the fitted c is smaller than the above mentioned lower bound. Using this η^* motivated lower bound on c, our final fitted c range in the LH parameter set becomes $0.149^{+0.103}_{-0.029}$. This range is also compatible with the other existing ones in the literature

[9,44]. We would also like to comment here that the error in our fitted c value can be reduced further once we have narrower error bands for the LQCD data on $\Sigma_u - \Sigma_d$ and thus further improving our estimation of c.

After fitting c to $T = 0$ results for the splitting between the u and d condensate values, we use the model to analyze the average condensate and the splitting as a function of T and eB. These results are summarized in Secs. III C 1 and III C 2. We found, like Ref. [33], that within the error band of $\langle \bar{\psi}\psi \rangle^{1/3}$ IMC is obtained for the condensates near the lower edge of the range. Furthermore, we observed that within the error band of F_π to get a better match with the phase diagram given by LQCD [15], one needs to consider F_π towards the upper edge of the range.

We further test our model by calculating the topological susceptibility (χ_t) and comparing that with the available LQCD results. We observed that with the fitted eB independent c value the model's prediction for χ_t at zero eB can produce the trend well as found in the lattice results [74,75]. Beyond T_{CO}, the quantitative mismatch with the lattice data may arise because of differences in the number of flavors in the two methods. For nonzero eB (for which, to our knowledge, there is no lattice study available for χ_t), we found that the χ_t increases as one increases the strength of the magnetic field up to the crossover temperature. This conclusion is similar to what is found in Ref. [52]. We also observed that, in the present model, χ_t's for different values of eB fall on top of that at zero eB once we go beyond the crossover temperature and the IMC effect is reflected. All these observations can be understood following the correlation between topological susceptibility and condensate average, as we know that the condensate is responsible for spontaneously breaking $U(1)_A$ symmetry along with the chiral symmetry. This connection is well reflected in the present study. All these predictions for nonzero eB could be further tested in future when lattice data becomes available for the same.

One natural extension of our study is the analysis of $2 + 1$ flavor QCD. The $U(1)_A$ breaking term, in this case, is of dimension 9 and the strength of the interaction is well known to be related to the $\eta - \eta'$ mass splitting [45,46]. It will be interesting to see whether the results for $\Sigma_u - \Sigma_d$ for finite eB at both 0 and finite T can be adequately described by the $2 + 1$ flavor model, or other terms in the effective models are necessary.

More recently, a magnetic field dependent 't Hooft interaction strength for three flavor [77] has been considered. All these facts validate our choice of considering arbitrary strength of 't Hooft interaction in presence of a magnetic field. In principle, c can also depend on eB as well as T, though we do not see evidence of a strong dependence on these variables in the range we consider.
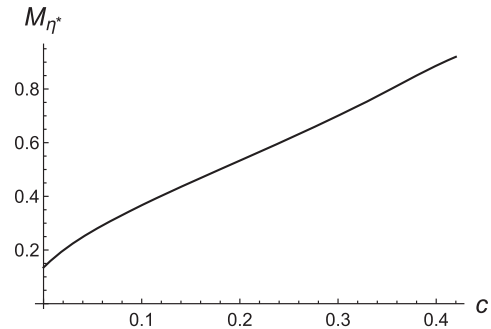

FIG. 11. η^* mass as a function of c for the CC parameter set.

However, a closer analysis of these effects will be interesting.

APPENDIX A: M_{η^*} VS c

In Fig. 11, we show the plot of η^* mass as a function of c for the CC parameter set. The plot is not very sensitive to the choice of parameter set (Table I) in the range shown. It is also to be noted that η^* and π^0 become degenerate at $c = 0$.

APPENDIX B: ANALYSIS WITH ANOTHER SET OF LQCD DATA

We tried to perform the whole analysis with another set of LQCD data [49] (referred to as Brandt13 in the text), which has a higher central value of condensate $(\langle \bar{\psi}_f \psi_f \rangle^{1/3} = 261$ MeV).[3] This value is at a renormalization

---

[3]It is to be noted here that the central value of the condensate in Brandt13 is roughly 20 MeV higher than that of JLQCD. This difference could be attributed to the systematic controls for LQCD discretization artifacts by continuum extrapolation and controls for finite-size effects in the former data set.

TABLE IV.   Central and the four corner parameter sets for LQCD data [49]. The quantities in the last four columns pertain to the nonlocal NJL model. As in the case of JLQCD, the condensate values are estimated at $\mu = 1$ GeV following the RG running shown in [68].

	$\langle \overline{\psi_f}\psi_f \rangle^{1/3}$ (MeV)	m_π (MeV)	F_π (MeV)	$F_{\pi,0}$ (MeV)	m (MeV)	G_0 (GeV)$^{-2}$	Λ (MeV)
Parameter set CC	244.7	135	90.0	86.28	4.89	28.03	814.75
Parameter set HH	256.9	135	98.25	95.40	5.04	31.35	809.04
Parameter set HL	256.9	135	81.75	74.90	3.54	15.01	1012.84
Parameter set LH	232.5	135	98.25	96.52	6.71	78.19	627.60
Parameter set LL	232.5	135	81.75	76.80	4.71	25.34	821.43

scale $\mu = 2$ GeV. To be able to use it in the present effective model scenario, we have evaluated it at $\mu = 1$ GeV following the procedures given in [68] as given in Table IV along with the corner parameter sets, which are obtained using the errors in the values of both the condensate $[\langle \bar{\psi}\psi \rangle^{1/3} = 261(13)(1)$ MeV] and the decay constant $[F_\pi = 90(8)(2)$ MeV]. Apart from the condensate, we also have the values for m_π and F_π, which are used to estimate the model parameters m, G_0, and Λ.

We follow here the same procedures as we did for the JLQCD data set. We explore all the data sets, including the corner ones, and look for the data set which could reproduce the IMC effect satisfactorily as compared to the LQCD data [16].

Looking at the Fig. 12, we observe that for Brandt13 LH, (232.5,98.25) is the lone parameter set that can replicate the IMC effect, quite satisfactorily. Then we move to the second part of our analysis, in which we look at the fitted c values (Table V) corresponding to the IMC reproducing parameter set(s). In this case, the fitted c value is -0.0255 for LH.

Now evoking the η^* related phenomenological argument as given in the main text before Eq. (53), where the plausible range of c is given as $c \in (0.12, 0.5]$, we can exclude the LH parameter set of Brandt13 data as a favorable one for the present model. Thus, we conclude that from Brandt13 data set [49], we do not find any
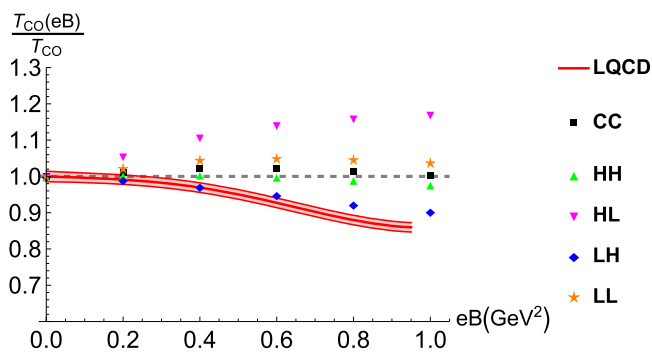
TABLE V. χ^2 fitting of condensate difference in c for all the five parameter sets from Brandt13 [49].

	c	χ^2 per d.o.f.
Parameter set CC	0.0749	0.334
Parameter set HH	-0.0198	6.076
Parameter set HL	0.2200	0.461
Parameter set LH	-0.0255	2.753
Parameter set LL	0.338	0.157

suitable parameter set for the present model, which can be reliably explored.

APPENDIX C: c DEPENDENCE OF χ_t IN THE LH PARAMETER SET OF JLQCD

In Fig. 13, we show the topological susceptibility as a function of the parameter c for different values of T at zero eB in the LH parameter set of JLQCD [48]. For a fixed eB, the topological susceptibility is 0 for $c = 0$ and rises as we increase c from 0. This rise is very sharp for smaller values of c and saturates very fast, particularly for the low-temperature values. Thus, a smaller c value will not be able to reproduce the expected result for χ_t. This gives us another reason, although in the hindsight, to exclude any parameter set which offers a smaller fitted c value and corroborates our choice of excluding the HH parameter set (for which the fitted central c value is 0.044) from η^* phenomenology.

FIG. 12.   The phase diagram in $T - eB$ plane for all parameter sets of Table IV (Brandt13 [49]) along with that as given by LQCD [15].
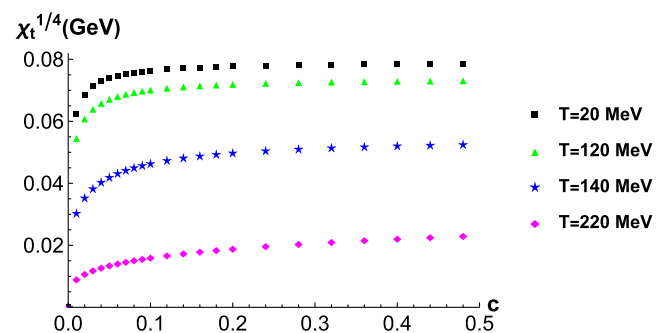

FIG. 13. χ_t as a function of the explicit $U(1)_A$ symmetric breaking parameter c at different temperatures for the LH parameter set of JLQCD [48].

[1] *Strongly Interacting Matter in Magnetic Fields*, edited by D. Kharzeev, K. Landsteiner, A. Schmitt, and H.-U. Yee (Springer, Heidelberg, Germany, 2013), Vol. 871.

[2] V. Skokov, A. Illarionov, and V. Toneev, Int. J. Mod. Phys. A **24,** 5925 (2009).

[3] K. Tuchin, Phys. Rev. C **93,** 014905 (2016).

[4] J. M. Lattimer and M. Prakash, Phys. Rep. **442,** 109 (2007).

[5] S. Schramm, B. Muller, and A. J. Schramm, Mod. Phys. Lett. A **07,** 973 (1992).

[6] V. Gusynin, V. Miransky, and I. Shovkovy, Nucl. Phys. **B462,** 249 (1996).

[7] D. Lee, C. N. Leung, and Y. Ng, Phys. Rev. D **55,** 6504 (1997).

[8] E. S. Fraga and A. J. Mizher, Phys. Rev. D **78,** 025016 (2008).

[9] J. K. Boomsma and D. Boer, Phys. Rev. D **81,** 074005 (2010).

[10] R. Gatto and M. Ruggieri, Phys. Rev. D **83,** 034016 (2011).

[11] B. Chatterjee, H. Mishra, and A. Mishra, Phys. Rev. D **84,** 014016 (2011).

[12] G. N. Ferrari, A. F. Garcia, and M. B. Pinto, Phys. Rev. D **86,** 096005 (2012).

[13] M. Ferreira, P. Costa, D. P. Menezes, C. Providência, and N. Scoccola, Phys. Rev. D **89,** 016002 (2014); **89,** 019902(A) (2014).

[14] M. D'Elia, S. Mukherjee, and F. Sanfilippo, Phys. Rev. D **82,** 051501 (2010).

[15] G. Bali, F. Bruckmann, G. Endrodi, Z. Fodor, S. Katz, S. Krieg, A. Schafer, and K. Szabo, J. High Energy Phys. 02 (2012) 044.

[16] G. Bali, F. Bruckmann, G. Endrodi, Z. Fodor, S. Katz, and A. Schafer, Phys. Rev. D **86,** 071502 (2012).

[17] G. Endrodi, J. High Energy Phys. 07 (2015) 173.

[18] M. D'Elia, F. Manigrasso, F. Negro, and F. Sanfilippo, Phys. Rev. D **98,** 054509 (2018).

[19] G. Endrodi, M. Giordano, S. D. Katz, T. Kovács, and F. Pittler, J. High Energy Phys. 07 (2019) 007.

[20] J. Chao, P. Chu, and M. Huang, Phys. Rev. D **88,** 054009 (2013).

[21] R. Farias, K. Gomes, G. Krein, and M. Pinto, Phys. Rev. C **90,** 025203 (2014).

[22] M. Ferreira, P. Costa, O. Louren co, T. Frederico, and C. Providência, Phys. Rev. D **89,** 116011 (2014).

[23] A. Ayala, M. Loewe, A. J. Mizher, and R. Zamora, Phys. Rev. D **90,** 036001 (2014).

[24] A. Ayala, M. Loewe, and R. Zamora, Phys. Rev. D **91,** 016002 (2015).

[25] E. Ferrer, V. de la Incera, and X. Wen, Phys. Rev. D **91,** 054006 (2015).

[26] J. O. Andersen, W. R. Naylor, and A. Tranberg, J. High Energy Phys. 02 (2015) 042.

[27] L. Yu, J. Van Doorsselaere, and M. Huang, Phys. Rev. D **91,** 074011 (2015).

[28] C. Providência, M. Ferreira, and P. Costa, Acta Phys. Pol. B Proc. Suppl. **8,** 207 (2015).

[29] N. Mueller and J. M. Pawlowski, Phys. Rev. D **91,** 116010 (2015).

[30] S. Mao, Phys. Lett. B **758,** 195 (2016).

[31] R. Farias, V. Timoteo, S. Avancini, M. Pinto, and G. Krein, Eur. Phys. J. A **53,** 101 (2017).

[32] D. Gómez Dumm, M. Izzo Villafañe, S. Noguera, V. Pagura, and N. Scoccola, Phys. Rev. D **96,** 114012 (2017).

[33] V. Pagura, D. Gomez Dumm, S. Noguera, and N. Scoccola, Phys. Rev. D **95,** 034013 (2017).

[34] Y. Nambu and G. Jona-Lasinio, Phys. Rev. **122,** 345 (1961).

[35] Y. Nambu and G. Jona-Lasinio, Phys. Rev. **124,** 246 (1961).

[36] R. Bowler and M. Birse, Nucl. Phys. **A582,** 655 (1995).

[37] R. S. Plant and M. C. Birse, Nucl. Phys. **A628,** 607 (1998).

[38] I. General, D. Gomez Dumm, and N. Scoccola, Phys. Lett. B **506,** 267 (2001).

[39] M. Praszalowicz and A. Rostworowski, Phys. Rev. D **64,** 074003 (2001).

[40] D. Gomez Dumm and N. N. Scoccola, Phys. Rev. D **65,** 074021 (2002).

[41] K. Kashiwa, Phys. Rev. D **83,** 117901 (2011).

[42] V. Ritus, Sov. Phys. JETP **48,** 788 (1978), http://cds.cern.ch/record/1060546.

[43] D. Gomez Dumm, A. Grunfeld, and N. Scoccola, Phys. Rev. D **74,** 054026 (2006).

[44] M. Frank, M. Buballa, and M. Oertel, Phys. Lett. B **562,** 221 (2003).

[45] S. Klevansky, Rev. Mod. Phys. **64,** 649 (1992).

[46] T. Hatsuda and T. Kunihiro, Phys. Rep. **247,** 221 (1994).

[47] S. Aoki *et al.* (Flavour Lattice Averaging Group Collaboration), Eur. Phys. J. C **80,** 113 (2020).

[48] H. Fukaya, S. Aoki, S. Hashimoto, T. Kaneko, H. Matsufuru, J. Noaki, K. Ogawa, T. Onogi, and N. Yamada (JLQCD), Phys. Rev. D **77,** 074503 (2008).

[49] B. B. Brandt, A. Jüttner, and H. Wittig, J. High Energy Phys. 11 (2013) 034.

[50] A. Bazavov *et al.* (HotQCD Collaboration), Phys. Rev. D **86,** 094503 (2012).

[51] Z.-Y. Lu and M. Ruggieri, Phys. Rev. D **100,** 014013 (2019).

[52] A. Bandyopadhyay, R. L. Farias, B. S. Lopes, and R. O. Ramos, Phys. Rev. D **100,** 076021 (2019).

[53] T. Hell, S. Roessner, M. Cristoforetti, and W. Weise, Phys. Rev. D **79,** 014022 (2009).

[54] G. 't Hooft, Phys. Rev. D **14,** 3432 (1976); **18,** 2199(E) (1978).

[55] G. 't Hooft, Phys. Rep. **142,** 357 (1986).

[56] S. Weinberg, *The Quantum Theory of Fields* (Cambridge University Press, Cambridge, England, 1996), Vol. 2.

[57] L. Del Debbio, L. Giusti, and C. Pica, Phys. Rev. Lett. **94,** 032003 (2005).

[58] K. Fukushima, K. Ohnishi, and K. Ohta, Phys. Rev. C **63,** 045203 (2001).

[59] S. Weinberg, Phys. Rev. Lett. **40,** 223 (1978).

[60] O. Wantz and E. Shellard, Nucl. Phys. **B829,** 110 (2010).

[61] K. Fujikawa, Phys. Rev. D **21,** 2848 (1980); **22,** 1499(E) (1980).

[62] D. Boer and J. K. Boomsma, Phys. Rev. D **78,** 054027 (2008).

[63] J. K. Boomsma and D. Boer, Phys. Rev. D **80,** 034019 (2009).

[64] M. D. Schwartz, *Quantum Field Theory and the Standard Model* (Cambridge University Press, Cambridge, England, 2014).

[65] J. A. M. Vermaseren, S. A. Larin, and T. van Ritbergen, Phys. Lett. B **405**, 327 (1997).

[66] T. van Ritbergen, J. A. M. Vermaseren, and S. A. Larin, Phys. Lett. B **400**, 379 (1997).

[67] K. G. Chetyrkin, Phys. Lett. B **404**, 161 (1997).

[68] L. Giusti, F. Rapuano, M. Talevi, and A. Vladikas, Nucl. Phys. **B538**, 249 (1999).

[69] H. G. Dosch and S. Narison, Phys. Lett. B **417**, 173 (1998).

[70] J. Berges and K. Rajagopal, Nucl. Phys. **B538**, 215 (1999).

[71] V. Dmitrasinovic, Phys. Rev. C **53**, 1383 (1996).

[72] M. S. Ali, C. A. Islam, and R. Sharma, arXiv:2103.15849.

[73] V. Miransky and I. Shovkovy, Phys. Rev. D **66**, 045006 (2002).

[74] S. Borsanyi *et al.*, Nature (London) **539**, 69 (2016).

[75] P. Petreczky, H.-P. Schadler, and S. Sharma, Phys. Lett. B **762**, 498 (2016).

[76] S. Borsanyi, Z. Fodor, C. Hoelbling, S. D. Katz, S. Krieg, C. Ratti, and K. K. Szabo (Wuppertal-Budapest Collaboration), J. High Energy Phys. 09 (2010) 073.

[77] J. Moreira, P. Costa, and T. E. Restrepo, Phys. Rev. D **102**, 014032 (2020).